Mosher, D.C., Erbacher, J., and Malone, M.J. (Eds.)
Proceedings of the Ocean Drilling Program, Scientific Results Volume 207

3. Campanian through Eocene Magnetostratigraphy of Sites 1257–1261, ODP Leg 207, Demerara Rise (Western Equatorial Atlantic)[1]

Yusuke Suganuma[2] and James G. Ogg[3]

ABSTRACT

Ocean Drilling Program (ODP) Sites 1257–1261 recovered thick sections of Upper Cretaceous–Eocene oceanic sediments on Demerara Rise off the east coast of Surinam and French Guiana, South America. Paleomagnetic and rock magnetic measurements of ~800 minicores established a high-resolution composite magnetostratigraphy spanning most of the Maastrichtian–Eocene. Magnetic behavior during demagnetization varied among lithologies, but thermal demagnetization steps >200°C were generally successful in removing present-day normal polarity overprints and a downward overprint induced during the ODP coring process. Characteristic remanent magnetizations and associated polarity interpretations were generally assigned to directions observed at 200°–400°C, and the associated polarity interpretations were partially based on whether the characteristic direction was aligned or apparently opposite to the low-temperature "north-directed" overprint. Biostratigraphy and polarity patterns constrained assignment of polarity chrons. The composite sections have a complete polarity record of Chrons C18n (middle Eocene)–C34n (Late Cretaceous).

[1]Suganuma, Y., and Ogg, J.G., 2006. Campanian through Eocene magnetostratigraphy of Sites 1257–1261, ODP Leg 207, Demerara Rise (western equatorial Atlantic). *In* Mosher, D.C., Erbacher, J., and Malone, M.J. (Eds.), *Proc. ODP, Sci. Results,* 207, 1–48 [Online]. Available from World Wide Web: <http://www-odp.tamu.edu/publications/207_SR/VOLUME/CHAPTERS/102.PDF>.
[2]Paleogeodynamics Research Group, Geological Survey of Japan, AIST, 1-1-1 Central 7, Higashi, Tsukuba, Ibaraki, 305-8567, Japan.
y.suganuma@aist.go.jp
[3]Department of Earth and Atmospheric Sciences, Civil Engineering Building, Purdue University, 550 Stadium Mall Drive, West Lafayette IN 47907-2051, USA.

Initial receipt: 26 May 2004
Acceptance: 23 May 2005
Web publication: 14 March 2006
Ms 207SR-102

LOCATION, GENERAL STRATIGRAPHY AND PALEOMAGNETIC GOALS

Demerara Rise is a projection of the continental margin off the northeast coast of Surinam and French Guiana, South America, in depths deeper than 700 m. Ocean Drilling Program (ODP) Leg 207 employed coring in multiple holes at each site to obtain continuous records of the expanded sections of Albian–Oligocene strata (Erbacher, Mosher, Malone, et al., 2004) (Fig. F1). Sites 1257–1261 recovered nearly 5000 m of sediment along a depth transect at 1900–3100 meters below seafloor (mbsf). In addition to high-resolution records of the Late Cretaceous Ocean Anoxic Events, Paleocene/Eocene Thermal Maximum, and Eocene/Oligocene boundary, several stratigraphic intervals were characterized by cyclic sedimentation that appear to be responses to Milankovitch orbital cycles. These cyclic intervals were the focus of our detailed magnetostratigraphic studies.

F1. Bathymetric map, p. 20.

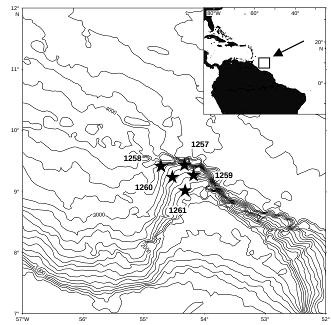

The generalized stratigraphy across the Demerara Rise consists of four main units:

1. Albian clay to sandstone overlain by Cenomanian–Santonian organic-rich “black shale;”
2. Campanian–Paleocene chalk with subtle oscillations in color and physical properties;
3. Eocene–lower Oligocene chalk to calcareous ooze with cyclic characteristics. Most sites have a major hiatus within the middle Eocene; and
4. Post-Oligocene deposition of primarily nannofossil ooze.

Magnetostratigraphy with constraints from biostratigraphy provides a chronostratigraphic framework in deep-sea sediments for paleoceanographic studies, including stable isotope trends and developing a high-resolution cyclostratigraphy tuned to orbital cycles. The primary goal of our paleomagnetic study was to establish a high-resolution magnetostratigraphy spanning the Late Cretaceous–Eocene at all Leg 207 sites with particular emphasis on continuous splices of cyclic sediments.

Note: for clarity in discussing calibrated chronostratigraphy vs. relative stratigraphic positions, we capitalize the official international subdivisions of epochs (e.g., Middle Eocene subepoch spans the Bartonian and Lutetian stages; Early Eocene subepoch is the Ypresian stage, etc.) The term “Lower” Eocene indicates the associated rock record that corresponds to the Early Eocene. Terms in lower case (“upper Eocene,” “lower Lower Eocene,” etc.). indicate only a relative position within the recovered strata of that international epoch or subepoch.

METHODS

Sampling

Shipboard magnetometer measurements were generally compromised by weak magnetizations, slurry intervals separating coherent blocks, and the inability to perform progressive thermal demagnetization. Therefore, we relied on extensive shore-based paleomagnetic and rock magnetic measurements of discrete samples.

Approximately 800 paleomagnetic minicores were collected from the Leg 207 sites. Cylindrical samples (12 cm^3) were cut using a water-cooled nonmagnetic drill bit attached to the standard drill press and trimmed with a diamond saw. The trimmed ends of such minicores were retained for analysis of carriers of magnetization. Shipboard sampling was generally at 3-m intervals from Hole B at each site. Guided by this initial magnetostratigraphic framework, additional postcruise sampling of selected priority intervals at ~1-m spacing was performed at the ODP Bremen core repository. This second set of detailed studies was designed to delimit the interpreted polarity reversals and to enhance the reliability of magnetostratigraphy from zones that had displayed relatively poor magnetic behavior.

Magnetic Measurement Procedures

Magnetic measurements for the main magnetostratigraphy program were carried out in the mu-metal-shielded facility at the Laboratory for Paleo- and Rock Magnetism at the Niederlippach complex of the Institut Für Allgemeine und Angewnandte Geophysik, Ludwig-Maximilians-Universität, Munich, Germany. The natural remanent magnetization (NRM) of each sample was measured using a cryogenic 2G Enterprises direct-current superconducting quantum interference device (DC-SQUID) magnetometer. The effective background noise of this three-axis cryogenic magnetometer for a minicore is ~1×10^{-6} A/m (1×10^{-3} emu/cm^3), which implies that reliable polarity information can be obtained from samples with remanent magnetizations as low as 4×10^{-6} A/m. To further increase the signal-to-noise ratio, we performed duplicate measurements whenever a sample had a remanent magnetization <8×10^{-6} A/m.

In order to remove secondary overprints and resolve the primary (characteristic) magnetization, we employed a combined treatment of alternating-field (AF) demagnetization to 5 mT followed by progressive thermal demagnetization in 30° or 50°C steps, typically from 150° to 450°C. The range and spacing of thermal steps depended upon the magnetic behavior displayed by suites of pilot samples from each lithology and stratigraphic age at each site. Magnetic susceptibility was monitored after each thermal demagnetization step >300°C to detect formation of new magnetic minerals or other anomalous changes in magnetic characteristics.

For visualizing the demagnetization behavior, computing characteristic directions, and assigning polarity ratings, we used the PALEOMAG software package, which has a combined graphical and analytical package designed for interpreting magnetostratigraphy and paleomagnetic statistics for large suites of samples (Zhang and Ogg, 2003; and as documented freeware available from Purdue University at **www.eas.purdue.edu/paleomag/**).

We conducted a separate study to investigate the nature of the remanence and the minerals responsible for stable remanence. A few representative specimens were selected based on differences of lithology and behavior of demagnetization characteristics through magnetic measurements for a set of rock magnetic experiments. These rock magnetic experiments were performed at the paleomagnetic laboratory of the Department of Environmental Sciences, Ibaraki University, Japan. The experiments included (1) progressive isothermal remanent magnetization (IRM) and (2) subsequent stepwise thermal demagnetization of acquired IRM.

MAGNETIC CHARACTERISTICS AND POLARITY ASSIGNMENTS

Generalized Rock Magnetic Behavior

Examples of typical magnetic behavior during combined AF and thermal demagnetization of the minicores are diagrammed in Figure F2. Nearly all samples displayed an NRM with positive inclination that is generally significantly steeper than the 20° inclination expected for the present latitude of the Leg 207 sites. A similar downward magnetic overprint is a common feature observed by ODP paleomagnetic studies and is considered to be induced during the downhole coring process (summarized in Acton et al., 2002).

F2. AF and thermal demagnetization samples, p. 21.

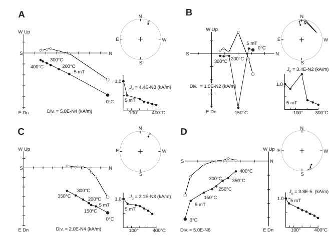

Upon reduction of this downward overprint using 5-mT AF demagnetization, most minicores displayed a relatively shallow inclination, low-temperature magnetic component that was gradually removed by progressive thermal demagnetization to ~200°C. As this low-temperature component was removed, the remanent magnetic directions generally either shifted slightly or else displayed a pronounced "hooklike" swing. As will be elaborated below, these two contrasting behaviors were utilized to assign magnetic polarity. During higher heating steps, the magnetic directions tended to be stable with a gradual loss of intensity—a trend toward the origin on vector plots—which permitted the isolation of a single component of magnetization.

Characteristic magnetization directions and associated variances were computed for each minicore by applying the least-squares three-dimensional line-fit procedure of Kirschvink (1980). The characteristic direction was visually assigned to the set of vectors that appeared to display removal of a single component in equal-area and vector plots during progressive demagnetization. The intensity of characteristic magnetization was computed as the mean intensity of those vectors used in the least-squares fit.

Curious Artifacts in Moist, Gray Minicores—Possible Goethite Formation?

In rare cases, some "fresh" minicores of relatively unoxidized gray facies that were still damp with the original pore water displayed a fascinating and temporary magnetodiagenetic artifact upon heating through an initial thermal demagnetization step of 150° or 200°C (see example in Fig. F2B). After this first heating step, the measured magnetic vector from these moisture-bearing cores (only the gray ones) was often offset from the main trend from initial NRM to the 5-mT AF step and through the higher heating steps. Even though the color of these minicores was generally lighter or bleached after the initial heating, there were no detectable changes in magnetic susceptibility. This behavior was never observed in minicores of the same lithologies that had experienced drying prior to the initial heating step; therefore we suspect that this curious artifact is a low-temperature alteration phenomenon. One possibility is that hydration of some of the reactive iron minerals (maybe iron sulfides?) occurred in these gray sediments to form a goethite-type mineral or similar low-susceptibility compound that acquired a spurious in-laboratory magnetic field upon the initial heating below 150°C but then later dehydrated or had exceeded its Curie point upon heating >200°C.

Diagenetic alternation of iron minerals upon sample storage was also observed in some Leg 207 cores sampled at the ODP repository at Bremen. In just 2 months, many intervals in these refrigerated sediments had already changed surface color from the original greenish gray to grayish tan. Neither the tannish altered minicores from the dark gray zones nor the dried (but still retaining the original gray color) minicores displayed the "anomalous 150°C directions." However, when this phenomenon was explained to some other paleomagnetists, they expressed skepticism about a goethite mineral being involved; therefore, we simply indicate this oddity of low-temperature thermal demagnetization of still-moist, fresh, gray sediments.

IRM and Magnetic Mineralogy Studies

Progressive direct magnetic fields up to 1.0 T were applied to typical light gray, dark gray, and reddish chalk to clayey chalk specimens from Hole 1258B (11 samples) and Hole 1259B (2 samples) in order to determine their IRM acquisition patterns (Fig. F3A).

F3. IRM acquisition, p. 23.

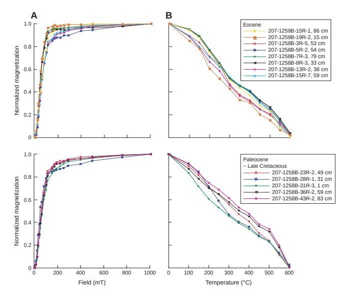

IRM values increase quickly and with relatively weak fields. Most specimens acquire more than 90% of their maximum IRM by 0.3 T and then display a slow increase to 1.0 T. The steep IRM acquisition curve below 0.3 T suggests the presence of a low-coercivity magnetic mineral in the sediments. A few specimens display a more continuous increase up to 1.0 T, which might be caused by a relatively higher concentration of a higher-coercivity mineral.

Subsequent stepwise thermal demagnetization of acquired IRM for all specimens displays a maximum unblocking temperature of ~600°C (Fig. F3B), which indicates that a dominant magnetic mineral is magnetite. A low-blocking-temperature component is also present, as suggested by the inflection point of the IRM demagnetization curves at 200°–350°C for several samples, which may indicate the presence of iron sulfides.

The rock magnetic experiments suggest that magnetite is an important carrier of magnetization in most sediments. We interpret that the characteristic magnetization (and polarity) carried by magnetite is indicative of the original primary magnetization acquired when the sediments were deposited.

Interpretation of Polarity Using Relative Declinations of Removed Vectors

Rotary drilling generally produces relative rotation between different sediment blocks within the core liner. In higher latitudes, one would rely on the stratigraphic clustering of positive or negative inclinations of the characteristic directions to assign normal polarity or reversed polarity zones, depending whether the site was known to be north or south of the paleoequator.

The Leg 207 sites are presently between 9° and 10°N latitude. Generalized global plate reconstructions generally indicate that South America has experienced a small amount of northward drift with negligible plate rotation since the Early Cretaceous (Chris Scotese, pers. comm. 2002); therefore, the pre-Oligocene paleolatitudes of the Leg 207 sites were projected to be within a few degrees of the paleoequator, and these reconstructions and independent compilations of South American paleomagnetic data were sometimes contradictory whether the Leg 207 sites would be north or south of that paleoequator. The near-equatorial paleolatitudes and uncertain northern vs. southern hemisphere positions through time implied that it would be inappropriate to assign polarity zones based solely on inclination patterns.

Therefore, we utilized the relative directions of low-temperature overprints (secondary magnetization) vs. the directions of higher-temperature characteristic magnetizations of the sediments to assist in interpreting the polarity of each minicore. The assumptions and procedure are detailed in Shipboard Scientific Party (2004a). This procedure is similar to that used by other paleomagnetists working with Deep Sea Drilling Project (DSDP) and ODP cores (e.g., Shibuya et al., 1991), who have demonstrated that relative orientation of overprints removed during progressive demagnetization can be used for identification of paleomagnetic polarity. The critical assumptions are that (1) an overprint vector of present-day north-directed polarity is superimposed on the original polarity vector, (2) there have not been major (>45°) tectonic rotations of the sites after sediment deposition, and (3) the relative declinations of the overprint vector and the underlying primary polarity vector can be deduced during progressive demagnetization. Ideally during progressive demagnetization, the north-directed vector of secondary magnetization (present-day magnetization) is removed, then the component of characteristic magnetization is resolved. If this characteristic magnetization also has normal polarity, then there would be only a minor change in magnetic declinations. However, if this characteristic magnetization is reversed polarity, then there would be a 180° rotation of declination. We called these two patterns "N-type" and the "hook-type," respectively.

For some intervals, the hook-type demagnetization plots enabled identification of the low-temperature secondary vector and the characteristic vector (e.g., Figs. F2E, F2F, F2G). By assigning the direction of this low-temperature component to be north (0° declination), we reoriented the characteristic vectors of the hook-type samples, which is a method also used by Shibuya et al. (1991). The clustering of these reoriented hook-type vectors toward "south" (180° declination) (Fig. F4) gives us renewed confidence in this procedure. However, isolation and resolution of secondary component vectors was generally not possible because either the last stages of their removal overlapped with onset of decreases in the intensity of the characteristic component or the few low-temperature demagnetization steps were inadequate to enable isolation or other behaviors during demagnetization (e.g., Figs. F2H, F2I, F2J). Of course, it is probable that there are a few erroneous assignments of polarity with this interpretation method. For example, a sample having only a reversed polarity characteristic direction without a significant secondary overprint might display a consistent linear decay upon demagnetization and be mistakenly assigned as N-type. Therefore, we do not trust the polarity interpretation of any single sample, but only the broader patterns. Approximately 80% of the minicore demagnetization behavior could be assigned as N-type or hook-type (sharp or curved), and these types were generally in stratigraphic clusters which we interpret as polarity zones.

A test of this method of polarity interpretation is possible in certain intervals that have biostratigraphic constraints on the possible primary polarity. For example, at all sites, the Paleocene/Eocene boundary occurred within an interval that was characterized by curved or sharp hook-type demagnetization paths. This is consistent with the placement of the Paleocene/Eocene boundary within the reversed polarity Chron C24r. Similarly, the Albian sediments displayed only N-type de-

F4. Magnetic behavior comparisons, p. 24.

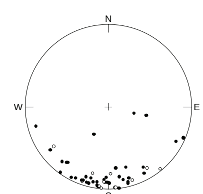

magnetization paths, which is consistent with their deposition within normal polarity Superchron C34n.

About 20% of the samples yielded uncertain polarities for a variety of reasons, including very weak magnetizations near the background noise level of the cryogenic magnetometer upon early stages of demagnetization, persistent steep downward-directed overprints, unstable magnetic directions, or ambiguous intermediate behavior between N-type and hook-type demagnetization paths.

Each characteristic direction was assigned a polarity and a qualitative reliability rating based upon its demagnetization behavior: (1) well-defined N or R directions computed from least-squares fits of at least three vectors; (2) normal polarity (NP) or reversed polarity (RP) directions computed from only two vectors or a suite of vectors displaying high dispersion but displaying clear polarity; (3) NPP or RPP samples that did not achieve adequate cleaning during demagnetization but their general N-type or hook-type behavior indicated the polarity; and (4) samples with uncertain N?? or R?? or indeterminate (INT) polarity that are not used to define polarity zones. To reduce the bias of a single observer, each of us made independent assignments of polarity and the selection and rating of characteristic magnetization vectors. In cases where the two paleomagnetists had different opinions, the samples were assigned a lower reliability rating.

Paleolatitudes

When both polarity and characteristic inclination are known for a discrete sample, its magnetic paleolatitude can be computed. The paleolatitude analyses and implications for South American plate reconstructions will be detailed in a separate publication, but the main results are summarized here.

The suites of discrete minicores revealed that the Leg 207 sites were at approximately 15°N latitude during the Albian ($\alpha95$ = 5°, k = 25), then progressively drifted southward to ~4°N during the Campanian–Maastrichtian (3.6°N, $\alpha95$ = 2.6°, k = 14) and Paleocene (4.4°N, $\alpha95$ = 2.5°, k = 19) and 1°S of the paleoequator during the early Eocene (1.5°S, $\alpha95$ = 0.7°, k = 51) and middle Eocene (1.0°S, $\alpha95$ = 0.7°, k = 82) (Suganuma and Ogg, unpubl. data). After the middle Eocene, there was a cumulative northward drift of ~10° to the present location of the sites. The general trends and projected paleolatitudes do not agree with published generalized global reconstructions (e.g., compilations by Alan Smith [in Gradstein et al., 2004] and Chris Scotese [2001, and www.scotese.com]). However, these paleolatitudes are consistent with some aspects of Apparent Polar Wander Path curves compiled for South America from local paleomagnetic studies combined with projections of selected North American and African paleomagnetic poles (e.g., Beck, 1998, 1999; Randall, 1998). A portion of this apparent disagreement between paleolatitudes computed from regional paleomagnetic data and those implied by global reconstructions may be an offset of the hotspot reference frame (used in global reconstructions) from the dipole reference frame (deduced from paleomagnetic analyses) and/or a "far-sighted" effect noticed in statistics of apparent poles from paleomagnetic data (A. Smith, pers. comm., 2003).

MAGNETOSTRATIGRAPHY

The standard geomagnetic timescale for the Late Cretaceous–Cenozoic is the "C-sequence" of marine magnetic anomalies and their calibration in other ODP-DSDP sites to foraminifer and nannofossil datums (e.g., Cande and Kent, 1992, 1995; Berggren et al., 1995). Characteristic portions of this pattern, when coupled with biostratigraphic constraints, generally enabled unambiguous correlations to the polarity zones recorded at Sites 1257, 1258, 1259, 1260, and 1261. For example, the relatively long reversed-polarity Chron C24r that spans the Paleocene/Eocene boundary could be confidently assigned to the reversed-polarity zone spanning this boundary at all sites. In sedimentary intervals deposited by fluctuating deposition rates or spanning rare interruptions by major hiatuses, the available biostratigraphic control was essential for proposing polarity chron assignments to the distorted pattern of polarity zones. Of course, it is inevitable that a few intervals among the array of sites had unreliable polarity interpretations or lacked biostratigraphic constraints which precluded unambiguous chron assignments. We have flagged uncertain chron assignments, but later revisions in biostratigraphy and/or methods of polarity determination may alter a few of the other assignments.

The following site-by-site summary of the Campanian–Eocene magnetostratigraphy is updated from our paleomagnetic sections in the site chapters within the Leg 207 *Initial Reports* volume (Erbacher, Mosher, Malone, et al., 2004). Paleomagnetism of the underlying Albian–Santonian at each site is merged into a concluding synthesis discussion.

Site 1257

Paleomagnetic analysis of minicores from combined Holes 1257A, 1257B, and 1257C revealed upper Chron C33n–C31r within a thick upper Campanian–lower Maastrichtian section, Chron C26n–C24r in an expanded upper Paleocene section, and portions of Chron C20r–C17n within a relatively condensed Middle Eocene interval (Shipboard Scientific Party, 2004b) (Fig. F5A).

F5. Magnetostratigraphy and characteristic directions, p. 25.

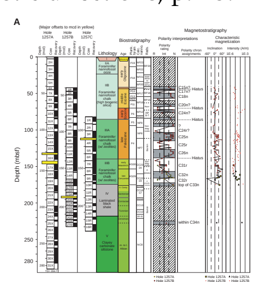

Campanian–Maastrichtian

When Campanian–Maastrichtian magnetostratigraphies from the three independent holes of Site 1257 are merged using the composite depth offsets, a consistent and simple polarity pattern emerges. The upper Campanian interval is constrained by foraminifer biostratigraphy to be uppermost Chron C33n–C32n (Fig. F5A). The early Maastrichtian age of the reversed polarity zone in the upper half of the succession implies an assignment to Chron C31r.

Late Paleocene–Early Eocene

The thick upper Paleocene yielded two major pairs of normal–reversed polarity zones, and their placement within foraminifer Zone P4 indicates an assignment to Chrons C26n-C25r-C25n-C24r. The base of this Paleocene section is a massive slump deposit, and its magnetization appears to have been acquired during redeposition in a normal polarity field, which was probably Chron C26n.

A compact, hiatus-delimited slice of Lower Eocene yielded primarily normal polarity, which may be Chron C24n. The apparent normal polarity of the uppermost Paleocene below the basal Eocene hiatus has no equivalent chron in the standard reference set (e.g., Cande and Kent, 1992), therefore may be an early Eocene remagnetization associated with the nondeposition interval or other artifact.

Middle and Late Eocene

A hiatus spanning a minimum of foraminifer Zones P7–P10 separates lower Eocene strata from the Middle Eocene unit. The relatively compact Middle Eocene greenish white foraminifer nannofossil chalk yields a relatively well defined suite of polarity zones. However, assignments of these zones to polarity chrons is inhibited by the low biostratigraphic resolution and apparent inconsistencies between currently available zonal identifications from the foraminifer and calcareous nannofossil assemblages and by gaps in core recovery. The limited stratigraphic control suggests that the basal polarity zones of this Middle Eocene segment might correspond to Chrons C20r–C20n and that the upper portion records Chrons C18r-C18n-C17r and the base of Chron C17n.

A thin Upper Eocene unit (foraminifer Zone P16) of normal polarity is bounded by disconformities between the underlying Middle Eocene (Zone P14) and overlying lower Oligocene (Zone P18) units. The only normal polarity chron within foraminifer Zone P16 is Chron C15n.

Site 1258

Paleomagnetic analysis of combined Holes 1258A, 1258B, and 1258C reveal Chrons C26r–C20r of the late Paleocene through the early Middle Eocene (Shipboard Scientific Party, 2004c) (Fig. F5B). Polarity chron assignments within the Campanian–Maastrichtian sediments are more ambiguous due to weak magnetizations but seem consistent with Chrons C33r–C29r of age. The high-resolution magnetostratigraphy of the relatively expanded Lower Eocene–lowermost Middle Eocene provides an important reference section for future cycle and isotope stratigraphy studies.

Campanian–Maastrichtian

The calcareous nannofossil clay to chalk of Campanian–middle Maastrichtian is characterized by very weak magnetic intensity. Many minicores were demagnetized to near the noise level of the cryogenic magnetometer upon heating >200°C, thereby introducing significant uncertainty in polarity interpretations. Clustering of normal and reversed polarity samples in both holes allowed identification of the main polarity zones (Fig. F5B), but assignment of polarity chrons is inhibited by the lack of detailed biostratigraphic constraints. The general pattern and age are consistent with the uppermost Chron C34n–C30n, but these tentative interpretations may be modified after further paleontological studies.

The uppermost Maastrichtian contains reddish brown chalk layers that display high magnetic intensities with NRMs dominated by normal overprints. Thermal demagnetization yielded reversed polarity in both Holes 1258A and 1258B, which is constrained by nannofossil Zone CC26 to be Chron C29r (Fig. F5B).

Paleocene

The greenish white foraminifer nannofossil chalk of the Paleocene is generally characterized by relatively weak intensity. The composite polarity zone pattern and foraminifer zonation of the merged holes is consistent with Chrons C26r-C26n-C25r-C25n-C24r (Fig. F5B), although the lowermost portion currently has a significant discrepancy between the foraminifer and the nannofossil age assignments.

Lower and Middle Eocene

The greenish white foraminifer nannofossil chalk that dominates the Eocene succession yields a relatively well defined suite of polarity zones (Fig. F5B). A reddish brown chalk that spans the Lower Eocene (Ypresian)–Middle Eocene (Lutetian) at ~40–100 meters composite depth (mcd) has strong magnetic intensity with a relatively steep downward-directed magnetic inclination. Thermal demagnetization >150°C of this reddish brown chalk was very effective in removing this downward overprint, and univectorial characteristic directions are from 250° through 400° or 450°C. Polarity chron assignments are based on average paleontological ages. The reversed polarity zone at the Paleocene/Eocene boundary must be Chron C24r; therefore, the overlying normal polarity zone is Chron C24n. The assignment of Chron C23n to the normal polarity zone at ~100 mcd is dictated by its position in the upper portion of foraminifer Zone P7. This implies that the narrow reversed polarity zone underlying Chron C23n in both holes must be a relatively condensed record of Chron C23r. The uppermost zone of reversed polarity within nannofossil Zone NP15 is constrained to be Chron C21r, and the underlying polarity pattern and biostratigraphic constraints are consistent with Chrons C22n and upper C22r.

However, there is an inconsistency in the interpreted polarity patterns between Holes 1258A and 1258B after adjusting to a composite meter depth scale in the interval between lower Chron C23n (~100 mcd) and Chron C22n (~50 mcd) (Fig. F5B). First, the top of polarity Chron C23n is offset between the two holes. Fault displacements that caused apparent relative removal of ~20 m of stratigraphic section between holes (shown by yellow squares in Fig. F5B) were assigned from shipboard comparisons of sedimentary features, biostratigraphic datums vs. depth, and other inconsistencies in the composite stratigraphy of the Paleocene–Early Eocene. An offset in the shipboard assignment of the foraminifer Zone P8/P7 boundary near the top of this distorted Chron C23n suggests the possibility of another unrecognized fault in Hole 1258A, which may have truncated uppermost Chron C23n in Hole 1258B and/or truncated the overlying Chron C22r in Hole 1258A. More worrisome is the interval of apparent normal polarity at ~80 mcd at each site, which, being between our assignments of Chron C22n and C23n, would seem to be in the middle of reversed polarity Chron C22r. There are at least two possible explanations for this "anomalous" normal polarity zone: (1) a stratigraphic interval within the reddish brown chalk characterized by a pervasive normal polarity overprint that was not effectively removed by our thermal demagnetization procedure, or (2) a duplication of a portion of the polarity pattern by another fault that could not be resolved from biostratigraphic constraints. Other than this annoying inconsistency within upper Chron C23n and lower Chron C22r, the Eocene polarity pattern is well resolved.

Site 1259

Paleomagnetic analysis of minicores from combined Holes 1259A and 1259B resolved numerous magnetic polarity zones within the Campanian–Eocene section (Shipboard Scientific Party, 2004d) (Fig. F5C). Chrons C31r–C29r are assigned to the Maastrichtian succession, and a complete record of Chrons C23n–C18r is resolved in the strata spanning late Early Eocene–Middle Eocene. This is one of the rare sites with a continuous magnetostratigraphy spanning the boundary interval between Early Eocene and Middle Eocene—a time span that is typically represented as a hiatus in most marine sections.

Campanian–Maastrichtian

The greenish gray chalk of upper Campanian–Maastrichtian is characterized by light–dark cycles. This interval was extensively sampled for postcruise paleomagnetic analyses for applying cyclostratigraphy to constrain the duration of the polarity chrons. The merged Maastrichtian polarity pattern from Holes 1259A and 1259B is consistent with Chrons C31r–C31n and C30n–C29r.

Paleocene

A ~25-m interval of negligible recovery within the upper Paleocene gray chalk and the extreme condensation of the lower Paleocene reddish brown chalk precludes reliable assignments of chrons to the observed polarity zones. If one assumes that the recovery gap had a similar sedimentation rate as the Lower Eocene, then it represents nonrecovery of Chron C25n and the underlying polarity pattern of the lower Upper Paleocene must be Chrons C26r-C26n-C25r.

Eocene

The uppermost Paleocene and lower Lower Eocene is weakly magnetized white chalk of predominantly reversed polarity, which is consistent with the expected Chron C24r at the Eocene/Paleocene boundary (Fig. F5C). Within Chron C24r, a thin normal polarity band is recorded in Core 207-1259A-37R—this and similar intra-C24r features at other sites are examined in the summary discussion.

An apparent hiatus in sedimentation during the middle Lower Eocene spans the time interval of foraminifer Zone P7, nannofossil Zone NP11 and portions of adjacent microfossil zones, and the associated Chrons C24n and C23r.

The upper Lower Eocene strata (foraminifer Zones P8–P9) display distinctive cycles of reddish brown–gray or dark–light green. Similarly to the coeval cyclic unit at Site 1258, hematite seems to be both the source of the reddish coloration and the carrier of a normal polarity overprint. Progressive thermal demagnetization was effective in resolving polarity zones, which are constrained by the biostratigraphy to be Chrons C23n-C22r-C22n.

The greenish white chalk facies of the lower Middle Eocene (foraminifer Zones P10 and P11) and upper Middle Eocene (foraminifer Zones P12–P14) have, respectively, very weak and moderate magnetic intensities (Fig. F5C). The pattern of well-defined polarity zones is constrained by biostratigraphy to be the complete succession of Chrons C21r–C18r and, possibly Chron C17r above a gap in recovery.

A narrow 10-m-thick zone of Late Eocene greenish gray chalk has relatively strong magnetization, and biostratigraphy (foraminifer Zone P16) constrains the dominance of normal polarity to be Chron C15n.

Site 1260

Closely spaced paleomagnetic sampling of combined Holes 1260A and 1260B produced a detailed record of Middle Eocene Chrons C21r–C18r (Shipboard Scientific Party, 2004e) (Fig. F5D). Lower-resolution sampling was adequate to identify Chrons C26n–C23n of the Late Paleocene and Early Eocene.

Campanian–Maastrichtian

Compared to other sites, the magnetostratigraphy of the Campanian–Maastrichtian was less successful. This white to greenish white chalk at Site 1260 displayed very weak magnetizations that generally approach the background noise level of the Munich cryogenic magnetometer upon heating >200°C. Very few minicores yielded reliable characteristic directions; and, especially in the Campanian, polarity assignments were also difficult (Fig. F5D). In addition, the biostratigraphic constraints are too broad to make assignments of polarity chrons to strata older than Chron C31n.

In contrast, the thermal demagnetization of the relatively strongly magnetized reddish brown chalk of the uppermost Maastrichtian effectively resolved reversed polarity Chron C29r.

Paleocene

Paleocene clayey nannofossil chalk is also characterized by weak magnetization, but it is significantly better than the underlying Campanian–Maastrichtian. No chron assignments were attempted in the relatively condensed lower Paleocene where biostratigraphic ages are inconsistent between foraminifer and nannofossil assignments. The upper Paleogene polarity pattern resolved by minicore analyses is constrained by biostratigraphy to represent Chron C26n through the lower portion of Chron C24r.

Lower and Middle Eocene

The clayey chalk of the earliest Eocene and reddish brown chalk of middle Early Eocene yielded a pattern of polarity zones that matches upper Chron C24r–lower C23n.

The lower Middle Eocene is also reddish brown chalk. Its polarity pattern fits uppermost Chron C22n–lower C21n (Fig. F5D). A hiatus spanning foraminifer Zone P9 and nannofossil Zone NP13 in the uppermost part of Core 207-1260A-1R apparently caused the juxtaposition of two normal polarity zones—uppermost Chron C22n directly overlies lower Chron C23n.

The upper Middle Eocene (~40–185 mbsf) mainly consists of greenish white foraminifer nannofossil chalk. The combined magnetostratigraphy of the two holes yielded a detailed polarity pattern identical to Chrons C21n–C18r, which is consistent with the paleontological ages.

Site 1261

Compared to other sites, Site 1261 is relatively condensed and the main successions of polarity chrons are bound by hiatuses (Shipboard Scientific Party, 2004f) (Fig. F5E). Chrons C31r–C29r (Maastrichtian), Chrons C27n–C24r (Paleocene–Early Eocene), and Chrons C21r–C19r (Middle Eocene) were resolved.

Campanian–Maastrichtian

As in Site 1260, the weakly magnetized Maastrichtian–Campanian greenish gray clayey chalk with light–dark cycles was commonly near the noise level of the Munich cryogenic magnetometer upon heating >200°C. Even though many of the individual-sample polarity interpretations are uncertain, when the data from the two holes are merged using composite depths, the generalized polarity zones and biostratigraphic constraints suggest Chrons C31r, C30n/C31n, and C29r (Fig. F5E).

Paleocene

Medium–light gray clayey chalk of the Paleocene has slightly stronger magnetizations than Late Cretaceous sediments. The upper Paleocene section contains the record of Chrons C27n–lower Chron C24r (Fig. F5E).

Eocene

Light greenish gray to medium gray chalk of Early–Middle Eocene age is very weakly magnetized, but the polarity of most samples was evident. The lowermost Eocene section at Site 1261 is entirely within Chron C24r, but is truncated by a hiatus that probably spanned Chrons C23r and C24n of middle Early Eocene. A second hiatus at the Early (Ypresian)/Middle (Lutetian) Eocene stage boundary spanned Chrons C22n and C22r. A sediment piece recovered from between these two hiatuses has normal polarity, and its biostratigraphic age suggests an assignment to Chron C23n.

Within the Middle Eocene, we resolved the complete succession of Chrons C20r-C20n-C19r and possibly portions of the underlying Chrons C21n and C21r. Above a sampling gap, the uppermost meters of the Middle Eocene yielded a dominance of normal polarity, and its age within with foraminifer Zones P13 and P14 indicates an assignment to Chron C18n.

MAGNETOSTRATIGRAPHIC CORRELATIONS AND THEIR IMPLICATIONS

Magnetostratigraphic correlations of all five sites are shown in Figure F6. In general, the magnetostratigraphy patterns, when coupled with biostratigraphic constraints, indicate that most sites of Leg 207 contain semicontinuous records of Chrons C18n–C27r of Middle Eocene to Late Paleocene age and Chrons C29r through potentially C33r of Maastrichtian–Campanian.

F6. Correlation of magnetostratigraphy, p. 30.

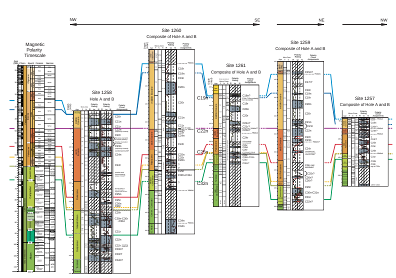

Aptian–Santonian

Cretaceous strata display progressive expansion toward the deeper sites. Although the pre-Campanian strata were not useful for magnetostratigraphy, owing to their deposition during the long normal polarity Superchron C34n, the paleomagnetism is important for determination of paleolatitudes.

Thermal demagnetization of clayey carbonate siltstone of Albian age at Site 1257 displays a relatively weak magnetization of normal polarity with positive inclination. Albian quartz siltstone of Site 1260 is characterized by relatively high intensity (~10^{-4}–10^{-3} A/m after 15-mT AF demagnetization) and high susceptibility. Progressive AF demagnetization of shipboard cores of Site 1260 siltstone indicated normal polarity with a mean inclination of +30°. Progressive thermal demagnetization of several minicores of this facies also yielded normal polarity with inclinations being uniformly positive.

The overlying black shale of the Cenomanian–Santonian at Site 1257 displayed the highest intensity magnetization (10^{-2}–10^{-1} A/m after 20-mT AF demagnetization using shipboard pass-through cryogenic magnetometer) of any facies at Site 1257. In contrast, this black shale unit at Site 1258 has magnetic intensities near the background noise level of the shipboard magnetometer. The positive inclinations that dominate the remanent magnetization of this black shale also indicate a paleolatitude north of the paleoequator. Of course, with any unit of entirely normal polarity, it possible that there is a contribution from a persistent overprint of present-day normal polarity (20° dipole inclination for Leg 207 sites). However, the fact that the mean inclinations of characteristic magnetization of Albian and Cenomanian paleomagnetic minicores are steeper than the present-day field is an indication that the Albian–Cenomanian paleolatitude was slightly northward of the present location of these sites. The Albian samples yield a paleolatitude of 15°N latitude ($\alpha95 = 5°$, $k = 25$) (Suganuma and Ogg, unpubl. data).

Campanian–Maastrichtian

Magnetostratigraphies of Campanian and Maastrichtian chalk from Sites 1257, 1258, 1259, and 1261 are consistent with assignments and correlations of Chrons C29r–C32n (Site 1260 had inadequate sampling and weak magnetizations that precluded useful polarity zone interpretations). However, until the array of sites have enhanced biostratigraphic studies to delimit microfossil datums, we caution that it is possible that portions of the current biostratigraphy polarity patterns at each site might have alternate assignments to polarity chrons. The expanded succession with duplicate magnetostratigraphic records from two holes at Site 1258 appears to have resolved the complete sequence of magnetic Chrons C29r–C34n. The Cretaceous/Paleogene (K/P) boundary impact event layer at Sites 1258, 1259, and 1260 is within polarity Chron C29r, as is expected from the reference magnetic polarity timescale.

Paleocene

At all sites, the Danian stage (Chrons C29r–C27n) is condensed and/or includes hiatuses. In contrast, the Upper Paleocene (Selandian and Thanetian stages) is present at all sites, and most holes yielded records of Chrons C26r–C24r. The distinctive Chron C26n provides a useful correlation marker among all sites. Magnetostratigraphic correlations and comparison to the reference magnetic polarity timescale suggest that relative sedimentation rates were variable within and among the sites, and minor hiatuses punctuate the record at some locations. For example, the relative widths of polarity zones associated with Chron C26n and overlying Chron C25r indicate relatively rapid deposition at Site 1257, where the early Paleocene is absent above the K/P boundary, whereas the coeval accumulation rates are significantly slower at sites where Paleocene sedimentation was initiated.

Eocene

Portions of the Eocene are significantly expanded at some sites. Site 1258 has a very thickened Early Eocene (Chrons C24r–C22n), and Sites 1259 and 1260 have a very thick Middle Eocene (Chrons C21r–C18r). At each site, the chron assignments are constrained by foraminifer and nannofossil biostratigraphy, but many portions also have a distinctive "fingerprint" match to the reference magnetic polarity timescale. A hiatus of variable duration occurs at Sites 1257, 1260, and 1261 between the Lower and Middle Eocene that removes the uppermost Lower Eocene (Chrons C22n and C22r; and an even longer time span at Site 1257). In contrast, the interpreted presence of Chron C22n and overlying Chron C21r at Sites 1258 and 1259 suggests a continuous record across this subepoch boundary.

A curious feature within the 2-m.y.-duration Chron C24r of latest Paleocene into Early Eocene are apparent thin normal polarity bands (e.g., at Site 1257 and Site 1258 within lower foraminifer Zone P6). Similar intra-C24r normal polarity subzones were interpreted in ODP Hole 1051A (Ogg and Bardot, 2001). Even though this apparent occurrence at multiple sites suggests that Chron C24r may include one or more short-duration normal polarity events that are not in the standard C-sequence model (Cande and Kent, 1992), we are hesitant to propose subchrons within Chron C24r without confirmation in a land-based section with fully oriented paleomagnetic data.

One major objective of our study is to provide a high-resolution magnetostratigraphic framework for a detailed cycle-stratigraphy analysis of the subtle facies oscillations and of the duration of polarity chrons and thereby estimation of the spreading rates for the corresponding marine magnetic anomalies. We successfully obtained expanded magnetostratigraphic record of Chrons C24r-C24n-C23r-C23n at Sites 1258 and 1260 and of Chrons C21r-C21n-C20r-C20n-C19r at Sites 1259, 1260, and 1261. This enables multiple sites to be used to verify the cycle-stratigraphy interpretations.

Although the Bartonian stage of the upper Middle Eocene (Chrons C18n–C17n) was recovered at four sites, assignment of the polarity zones to chrons was generally uncertain. The recovered strata of the Priabonian stage at Sites 1257 and 1259 on the northeast margin of Demerara Rise record only a brief portion of the Late Eocene Chrons C17n–C15n.

SUMMARY

Magnetostratigraphy of the five Leg 207 sites provides an enhanced chronologic control for the Latest Cretaceous–Eocene of Demerara Rise. Thermal demagnetization of ~800 minicores collected from the sites removed a downward-directed overprint induced during the drilling process and a low-temperature component that was effectively removed by heating >200°C. The magnetostratigraphy interpretations and biostratigraphic constraints at the five sites enabled identification and commonly a detailed delimiting of Chrons C18n–C27r of the Middle Eocene–Late Paleocene and of Chrons C29r–C31r of the Maastrichtian–Campanian.

ACKNOWLEDGMENTS

We thank the ODP staff and crews of the *JOIDES Resolution* for their help and good company during Leg 207. The weeks of a round-the-clock acquisition of magnetic measurements were only possible through the generosity of Professor Valerian Bachtadse and Manuela Weiss, who allowed us to monopolize the paleomagnetic facilities at the Institute of Geophysics at the University of Munich, Germany, and of Makoto Okada at the paleomagnetic laboratory of the Department of Environmental Sciences of the University of Ibaraki, Japan. The energetic group at the ODP Core Repository at Bremen sent us more than 100 additional minicores and then aided us for a 4-day race to drill-press an additional 300 minicores to improve resolution of magnetic reversal boundaries at the midpoint of our analysis marathon.

This research utilized samples and/or data provided by the Ocean Drilling Program (ODP). ODP is sponsored by the U.S. National Science Foundation (NSF) and participating countries under management of Joint Oceanographic Institutions (JOI), Inc. The JOI/U.S. Science Advisory Committee (USSAC) provided advance funding to J. Ogg and a special travel grant to accomplish the postcruise collection and analyses of the minicores in Germany.

REFERENCES

Acton, G.D., Okada, M., Clement, B.M., Lund, S.P., and Williams, T., 2002. Paleomagnetic overprints in ocean sediment cores and their relationship to shear deformation caused by piston coring. *J. Geophys. Res.,* 107. **doi:10.1029/2001JB000518**

Beck, M.E., Jr., 1998. On the mechanism of crustal block rotations in the central Andes. *Tectonophysics,* 299:75–92.

Beck, M.E., Jr., 1999. Jurassic and Cretaceous apparent polar wander relative to South America: some tectonic implications. *J. Geophys. Res.,* 104:5063–5067.

Berggren, W.A., Kent, D.V., Swisher, C.C., III, and Aubry, M.-P., 1995. A revised Cenozoic geochronology and chronostratigraphy. *In* Berggren, W.A., Kent, D.V., Aubry, M.-P., and Hardenbol, J. (Eds.), *Geochronology, Time Scales and Global Stratigraphic Correlation.* Spec. Publ.—SEPM (Soc. Sediment. Geol.), 54:129–212.

Cande, S.C., and Kent, D.V., 1992. A new geomagnetic polarity time scale for the Late Cretaceous and Cenozoic. *J. Geophys. Res.,* 97:13917–13951.

Cande, S.C., and Kent, D.V., 1995. Revised calibration of the geomagnetic polarity timescale for the Late Cretaceous and Cenozoic. *J. Geophys. Res.,* 100:6093–6095.

Erbacher, J., Mosher, D.C., Malone, M.J., et al., 2004. *Proc. ODP, Init. Repts.,* 207 [CD-ROM]. Available from: Ocean Drilling Program, Texas A&M University, College Station TX 77845-9547, USA. [**HTML**]

Gradstein, F.M., Ogg, J.G., and Smith, A. (Eds.), 2004. *A Geologic Time Scale 2004:* Cambridge (Cambridge Univ. Press).

Kirschvink, J.L., 1980. The least-squares line and plane and the analysis of palaeomagnetic data. *Geophys. J. R. Astron. Soc.,* 62:699–718.

Ogg, J.G., and Bardot, L., 2001. Aptian through Eocene magnetostratigraphic correlation of the Blake Nose Transect (Leg 171B), Florida continental margin. *In* Kroon, D., Norris, R.D., and Klaus, A. (Eds.), *Proc. ODP, Sci. Results,* 171B [Online]. Available from World Wide Web: <**http://www-odp.tamu.edu/publications/171B_SR/chap_09/chap_09.htm**>. [Cited 2004-05-20]

Randall, D.E., 1998. A new Jurassic–Recent apparent polar wander path for South America and a review of central Andean tectonic models. *Tectonophysics,* 299:49–74.

Scotese, C.R., 2001. PALEOMAP project. Available from World Wide Web: <**http://www.scotese.com**>. [Cited 2004-05-20]

Shibuya, H., Merrill, D.L., Hsu, V., and Leg 124 Shipboard Scientific Party, 1991. Paleogene counterclockwise rotation of the Celebes Sea—orientation of ODP cores utilizing the secondary magnetization. *In* Silver, E.A., Rangin, C., von Breymann, M.T., et al., *Proc. ODP, Sci. Results,* 124: College Station, TX (Ocean Drilling Program), 519–523.

Shipboard Scientific Party, 2004a. Explanatory notes. *In* Erbacher, J., Mosher, D.C., Malone, M.J., et al., *Proc. ODP, Init. Repts.,* 207 [Online]. Available from World Wide Web: <**http://www-odp.tamu.edu/publications/207_IR/chap_02/chap_02.htm**>. [Cited 2004-05-20]

Shipboard Scientific Party, 2004b. Site 1257. *In* Erbacher, J., Mosher, D.C., Malone, M.J., et al., *Proc. ODP, Init. Repts.,* 207 [Online]. Available from World Wide Web: <**http://www-odp.tamu.edu/publications/207_IR/chap_04/chap_04.htm**>. [Cited 2004-05-20]

Shipboard Scientific Party, 2004c. Site 1258. *In* Erbacher, J., Mosher, D.C., Malone, M.J., et al., *Proc. ODP, Init. Repts.,* 207 [Online]. Available from World Wide Web: <**http://www-odp.tamu.edu/publications/207_IR/chap_05/chap_05.htm**>. [Cited 2004-05-20]

Shipboard Scientific Party, 2004d. Site 1259. *In* Erbacher, J., Mosher, D.C., Malone, M.J., et al., *Proc. ODP, Init. Repts.,* 207 [Online]. Available from World Wide Web: <**http://www-odp.tamu.edu/publications/207_IR/chap_06/chap_06.htm**>. [Cited 2004-05-20]

Shipboard Scientific Party, 2004e. Site 1260. *In* Erbacher, J., Mosher, D.C., Malone, M.J., et al., *Proc. ODP, Init. Repts.,* 207 [Online]. Available from World Wide Web: <**http://www-odp.tamu.edu/publications/207_IR/chap_07/chap_07.htm**>. [Cited 2004-05-20]

Shipboard Scientific Party, 2004f. Site 1261. *In* Erbacher, J., Mosher, D.C., Malone, M.J., et al., *Proc. ODP, Init. Repts.,* 207 [Online]. Available from World Wide Web: <**http://www-odp.tamu.edu/publications/207_IR/chap_08/chap_08.htm**>. [Cited 2004-05-20]

Zhang, C., and Ogg, J.G., 2003. An integrated paleomagnetic analysis program for stratigraphy labs and research projects. *Comput. Geosci.,* 29:613–625.

APPENDIX

Demagnetization data (AF and thermal steps) of all 800 minicores with sample-by-sample summary comments on assignment of polarity and reliability to characteristic directions are shown in Tables AT1, AT2, AT3, AT4, AT5, AT6, AT7, AT8, AT9, AT10, and AT11.

Figure F1. Bathymetric map of Leg 207 drilling sites on Demerara Rise.

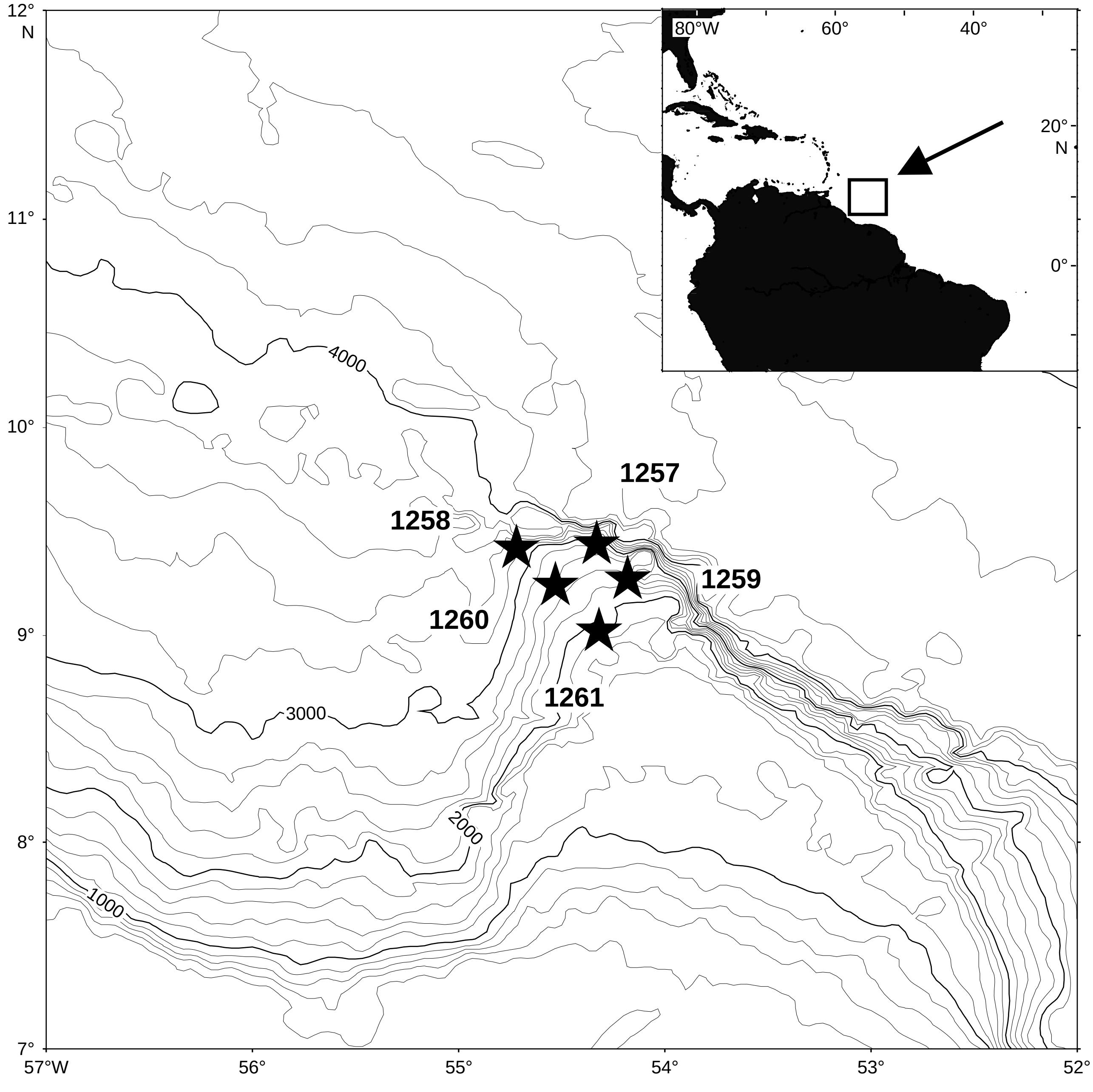

Figure F2. Examples of alternating-field demagnetization followed by progressive thermal demagnetization for selected samples. For each sample, the following are shown: an orthogonal vector plot with solid (open) symbols for data projected onto the horizontal (vertical) plane, a normalized plot of the intensity of magnetization vs. demagnetization step, and a stereographic projection. **A.** Section 207-1258B-8R-3, 33 cm (early Eocene; 72.96 mbsf) = N-type behavior, assigned as N, may represent brief normal zone within Chron C22r. **B.** Section 207-1258A-22R-3, 9 cm (late Paleocene; 223.62 mbsf) = N-type (150°C step is an artifact—see text), assigned as NP, within Chron C25n. **C.** Section 207-1260B-13R-1, 14 cm (early Eocene; 238.09 mbsf) = N-type behavior, assigned as N, within Chron C24n. **D.** Section 207-1261A-25R-1, 51 cm (middle Eocene; 410.81 mbsf) = N-type, assigned as N, within Chron C20n. (Continued on next page.)

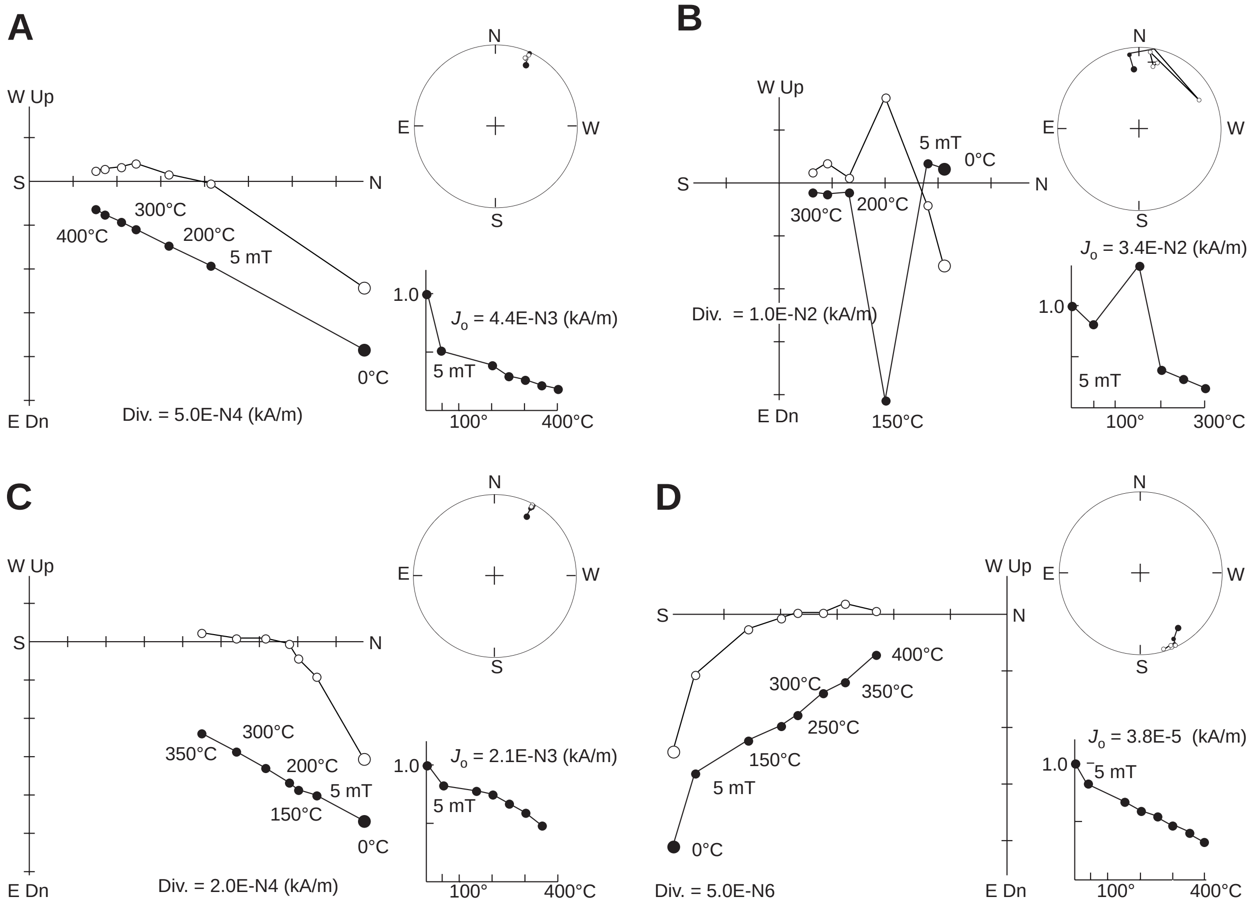

Figure F2 (continued). E. Section 207-1259A-26R-1, 13 cm (middle Eocene; 237.04 mbsf) = hook-type, assigned as R, within Chron C20r. **F.** Section 207-1260A-25R-7, 32 cm (early Eocene; 227.71 mbsf) = hook-type, assigned as R, within Chron C23r. **G.** Section 207-1261A-23R-3, 37 cm (middle Eocene; 394.47 mbsf) = hook-type, assigned as R, within Chron C19r. **H.** Section 207-1257B-4R-4, 84 cm (early Eocene; 71.84 mbsf) = quasi-hook-type (declination shifts by 50°), assigned as RP, within Chron C23r. **I.** Section 2071258A-28R-5, 67 cm (late Maastrichtian; 284.02 mbsf) = hook-type, but no endpoint reached, therefore assigned as RPP, within Chron C29r. **J.** Section 207-1259A-44R-3, 94 cm (late Paleocene; 415.51 mbsf) = hook-type, assigned as RP, within Chron C25r.

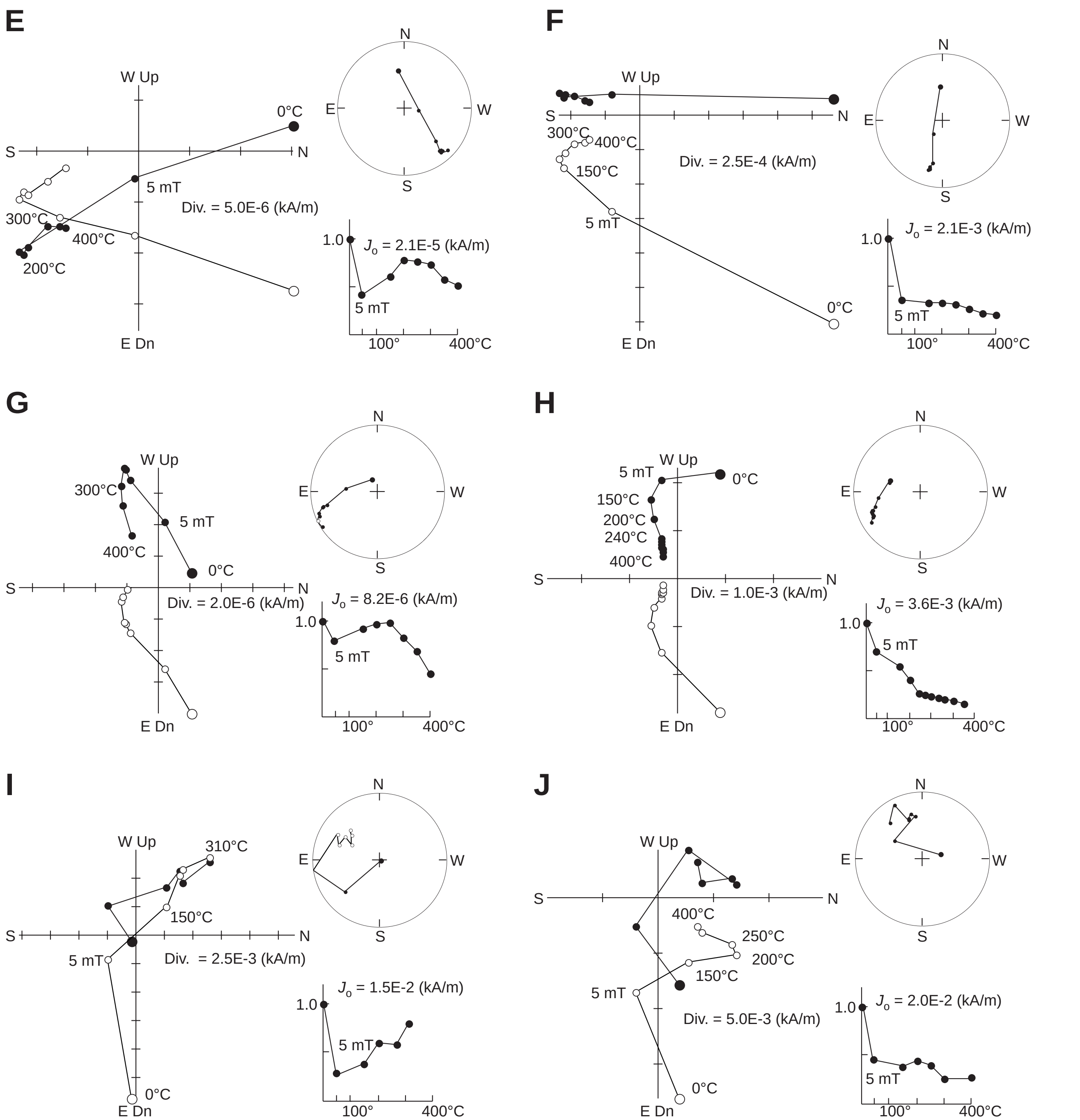

Figure F3. Acquisition of IRM and its thermal demagnetization of representative samples. **A.** Normalized IRM acquisition curves up to 1.0 T. **B.** Demagnetization of IRM up to 600°C.

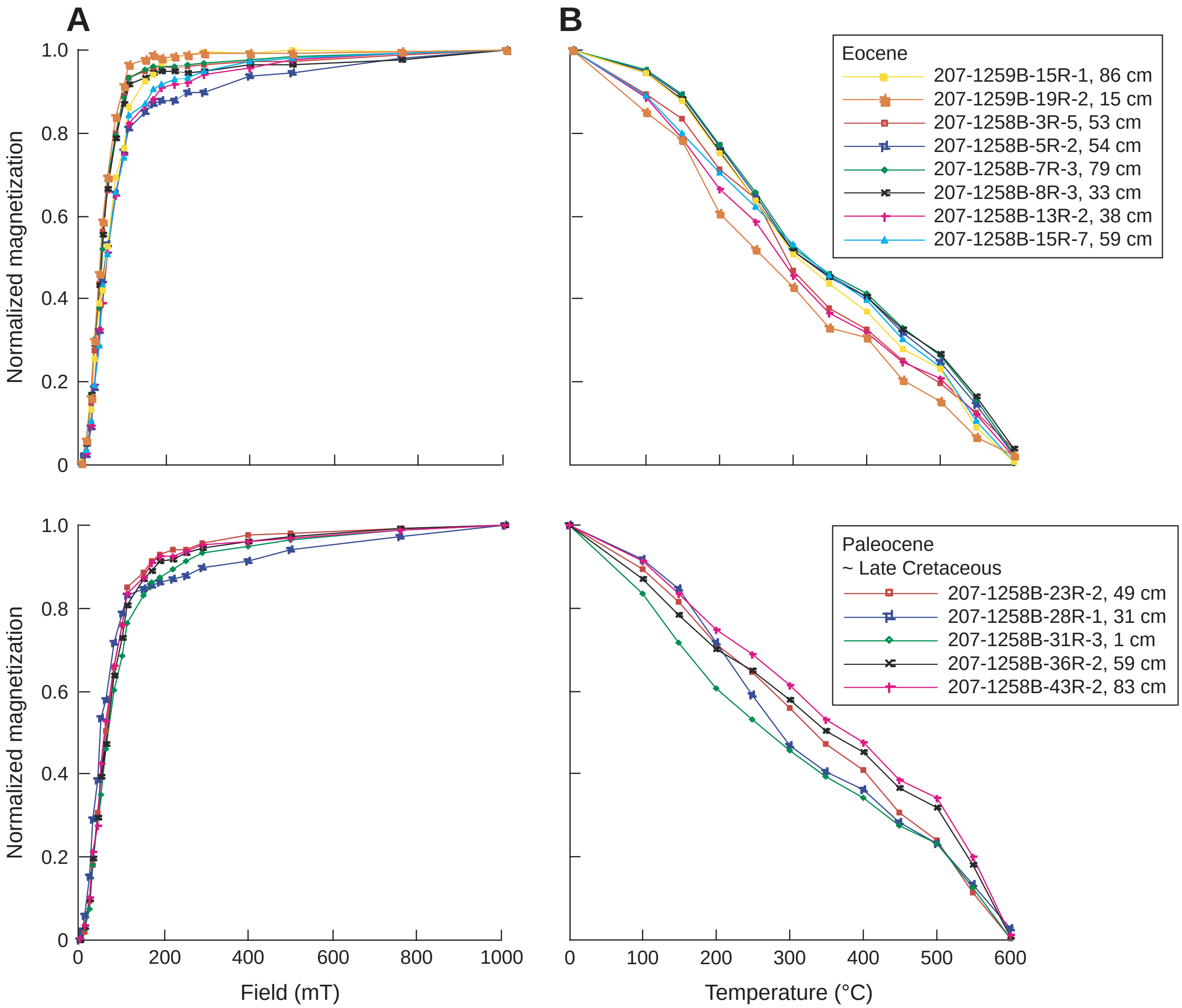

Figure F4. Comparison for hook-type magnetic behaviors of relative orientation of characteristic remanent magnetization (least-squares fit to higher temperature steps) to the low-temperature component (assigned as "North-oriented," declination 0°). We assumed that the low-temperature component is dominated by a secondary overprint of present-day field and that hook-type extreme shifts in declination upon demagnetization represented the removal of this normal polarity overprint from a characteristic reversed polarity magnetization. The clustering of higher-temperature directions toward south-directed declinations supports this interpretation. Therefore, even though it was not always possible to adequately resolve the orientation of the low-temperature vector in samples displaying similar hook-type demagnetization paths (e.g., Fig. F2E, p. 22), it is probable that these also are reversed polarity characteristic directions with a superimposed normal polarity secondary vector.

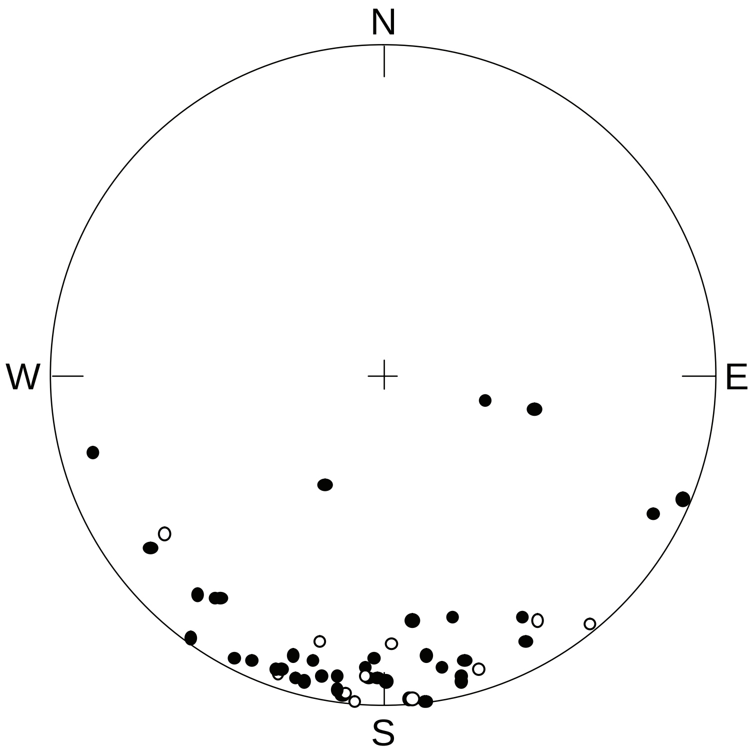

Figure F5. A. Magnetostratigraphy and characteristic directions from Eocene–Cretaceous in Holes 1257A, 1257B, and 1257C based on analysis of discrete samples. The majority of the minicores are from Hole 1257B, with enhanced Maastrichtian–Campanian from Holes 1257A and 1257C. The measured data from the three holes have been merged using the composite depth scale, and these adjustments are shown schematically for each hole (rightmost columns). Polarity ratings are graded according to reliability and number of vectors utilized in the characteristic direction (R = reliable reversed polarity, INT = indeterminate, N = reliable normal polarity; and relative placement of other points indicates degree of precision or uncertainty). Polarity zones are assigned according to clusters of individual polarity interpretations. Normal polarity zones = dark gray, reversed polarity zones = white, and uncertain polarity or gaps in data coverage = cross hatched. Assignments of polarity chrons are based on the polarity zone pattern and the constraints from microfossil biostratigraphy. (Continued on next four pages.)

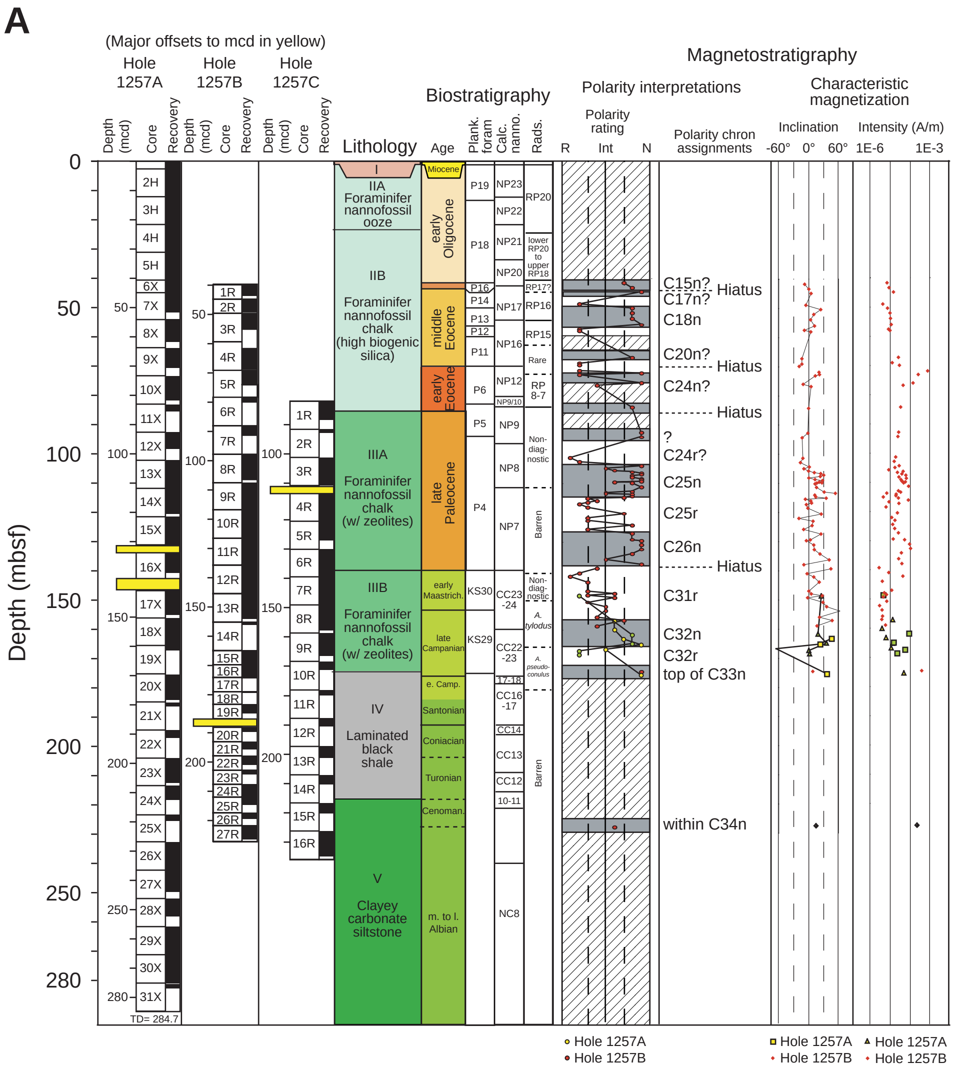

Figure F5 (continued). B. Holes 1258A and 1258B (Eocene–Cretaceous).

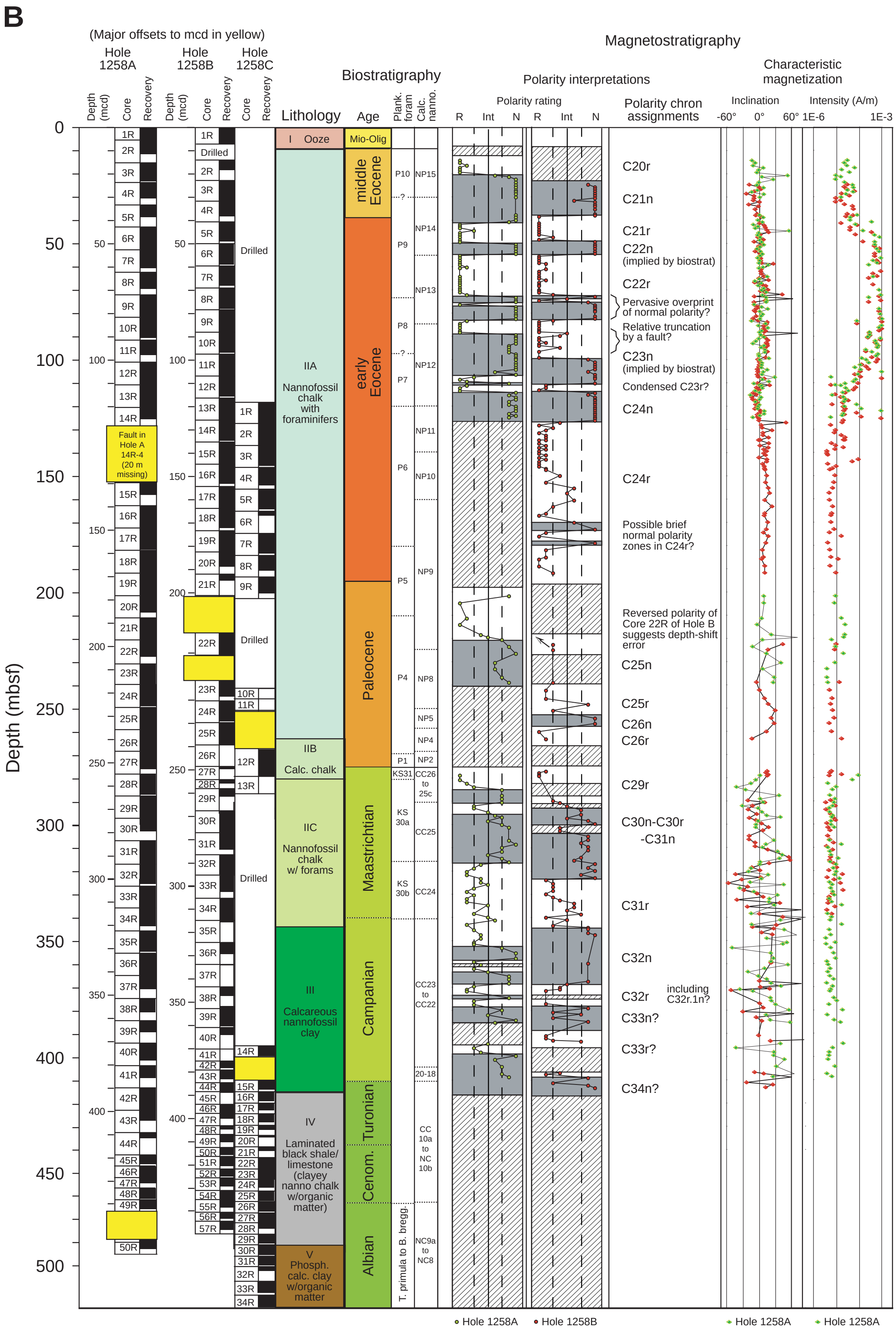

Figure F5 (continued). C. Holes 1259A and 1259B (Eocene–Cretaceous).

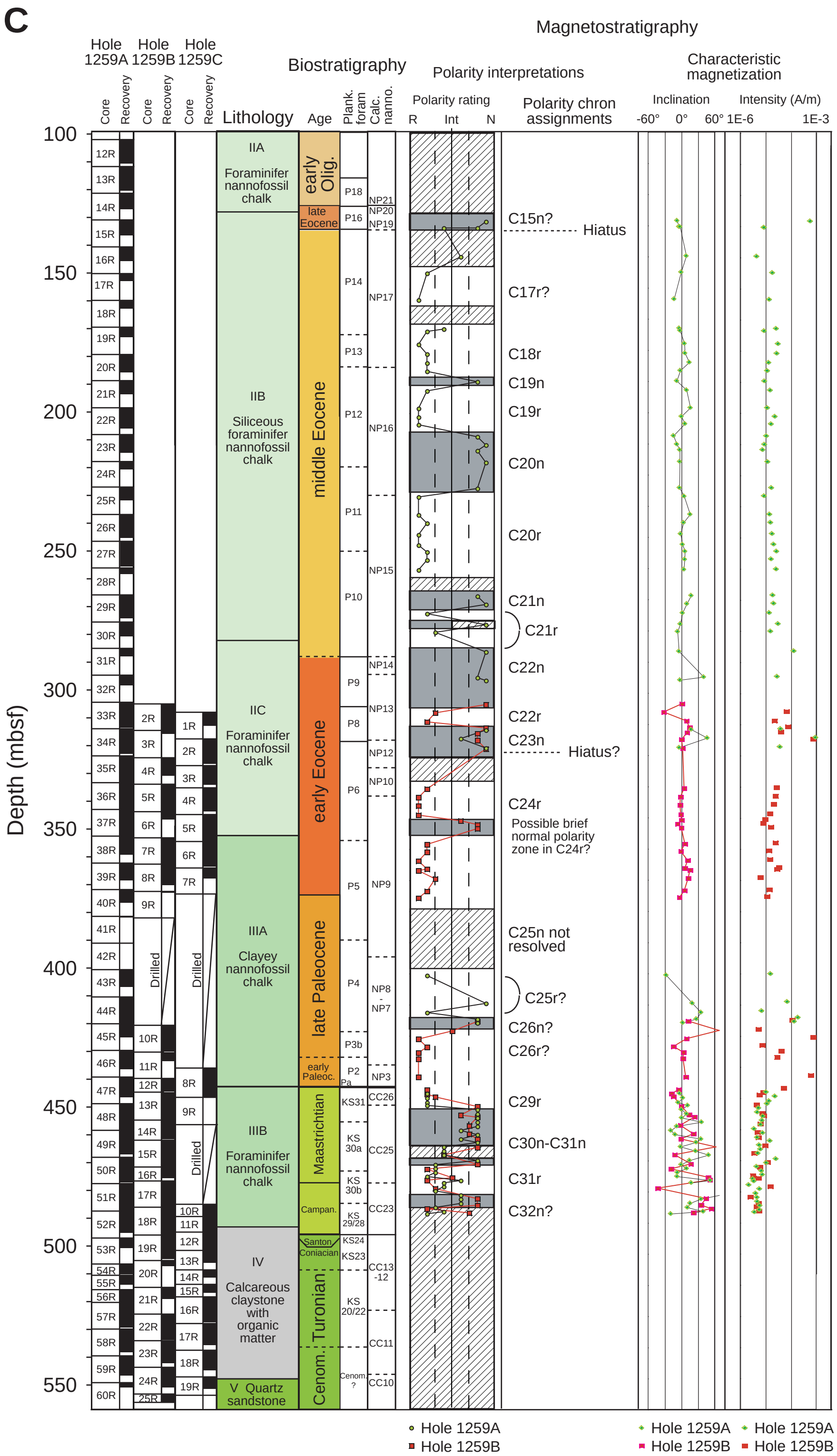

Figure F5 (continued). D. Holes 1260A and 1260B (middle Eocene–Campanian and Albian).

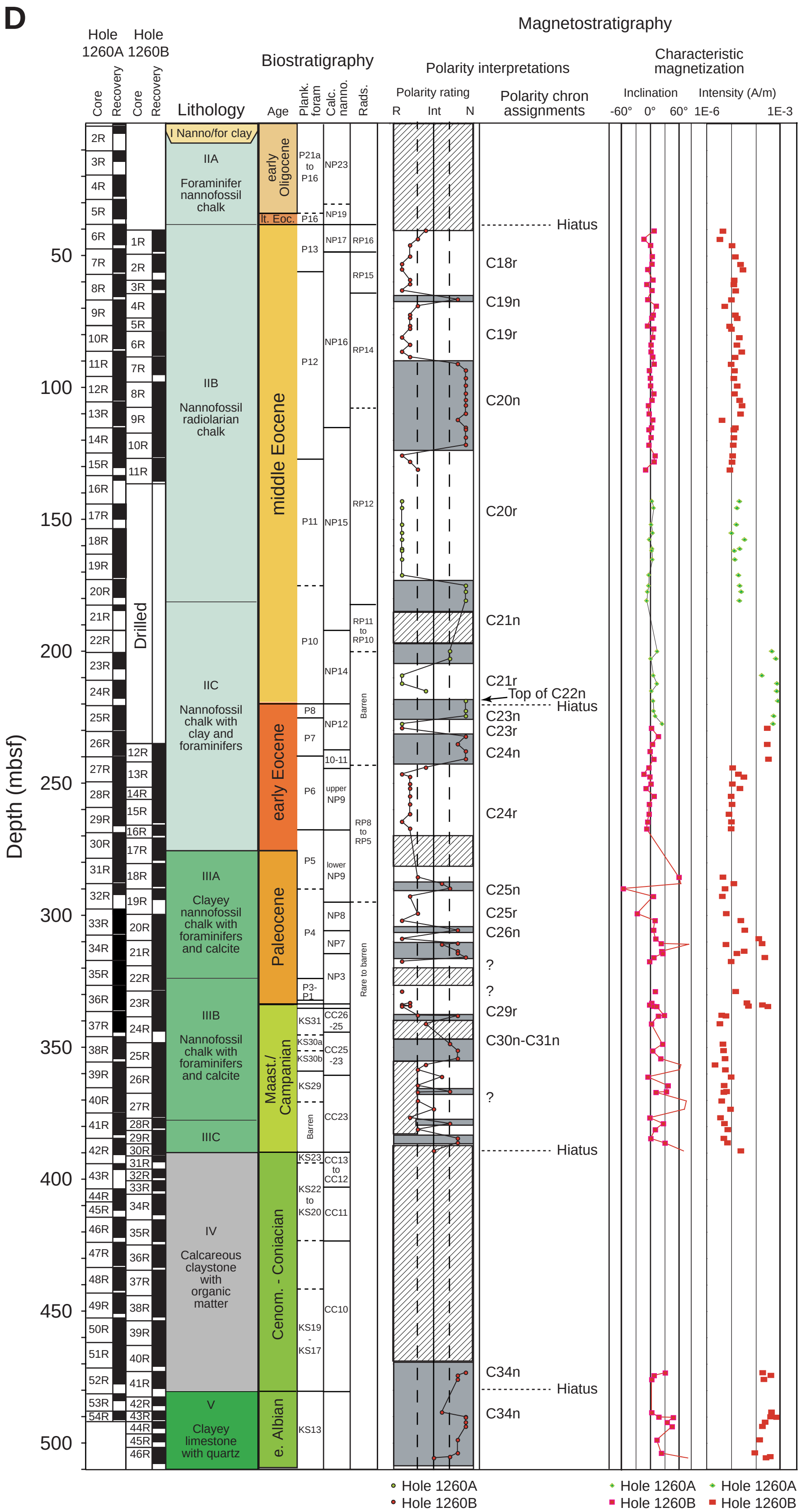

Figure F5 (continued). E. Holes 1261A and 1261B (middle Eocene–Campanian).

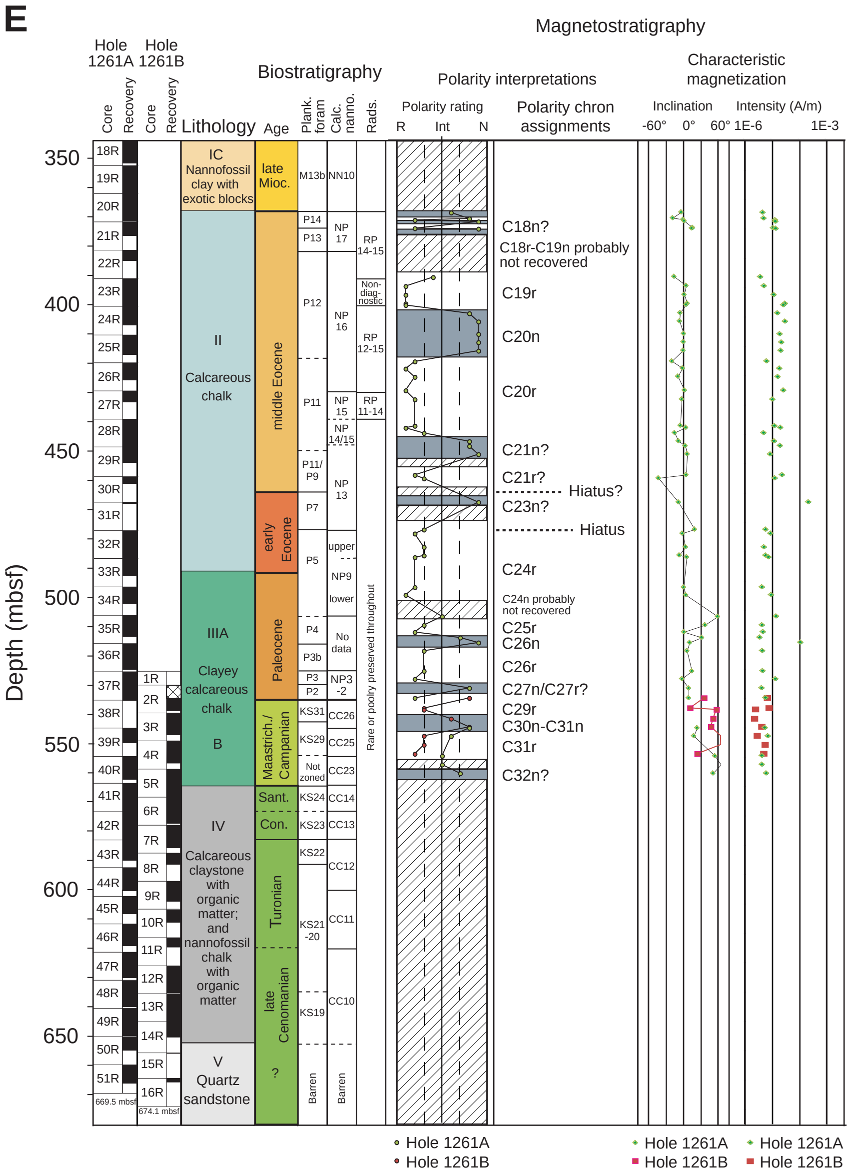

Figure F6. Correlation of magnetostratigraphy of Leg 207 sites on Demerara Rise. Selected magnetostratigraphic correlation horizons (colored lines) are near the stage boundaries of the Paleogene–Maastrichtian. Sites are aligned using polarity Zone C22n at the base of middle Eocene as the horizontal level. Magnetic polarity and biostratigraphic timescale is that used on Leg 207 (Shipboard Scientific Party, 2004). (This figure is available in an oversized format.)

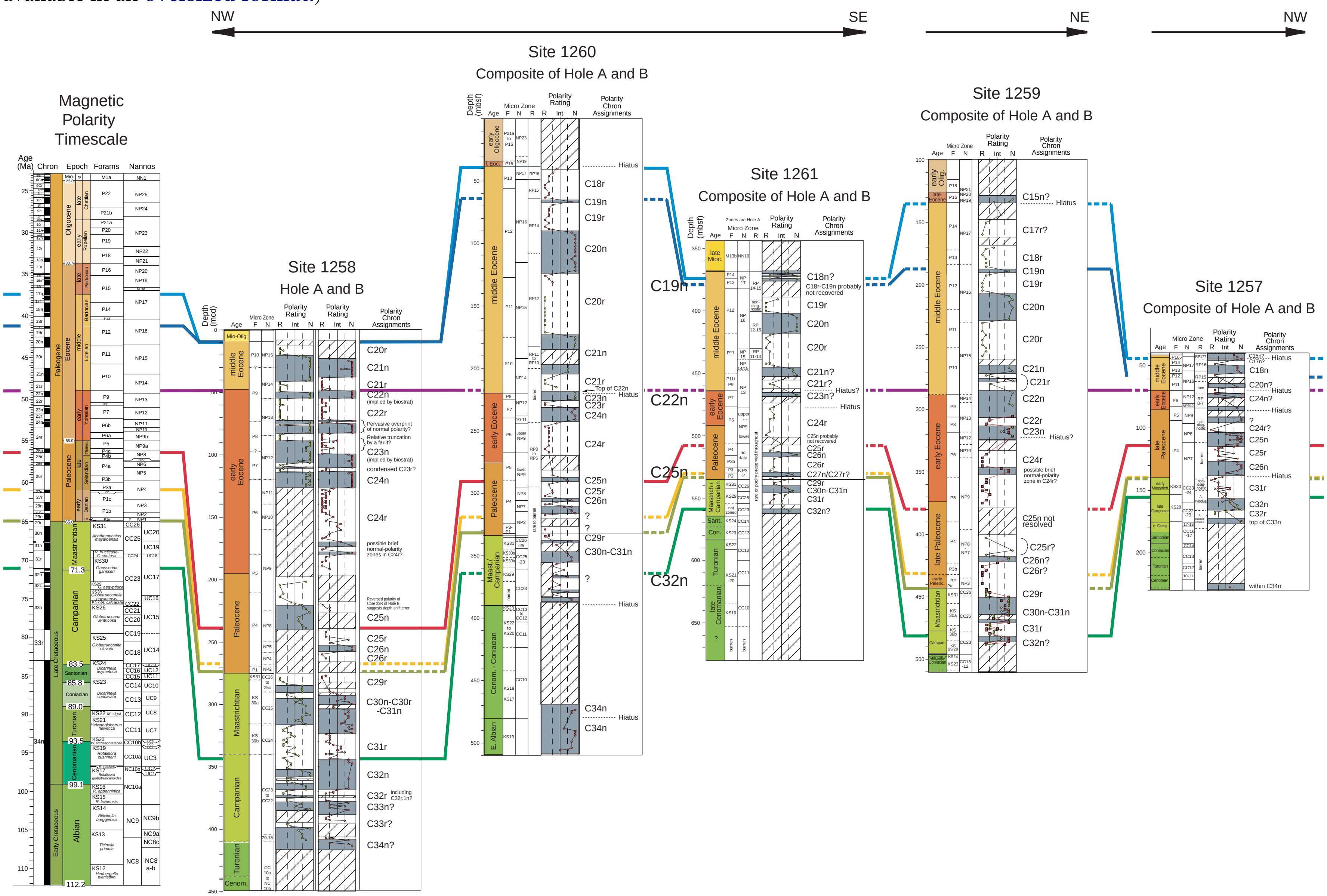

Table AT1. Early Maastrichtian to mid-Campanian paleomagnetic analysis, Hole 1257A. (See table notes. Continued on next page.)

Core, section, interval (cm)	Depth (mcd)	Demagnetization (mT/°C)	Declination (°)	Inclination (°)	ChRM intensity (mA/m)	Error	Polarity assignments	Comments
207-1257A-								
18X-1, 118	157.280							
		NRM 0	165.3	68.5	7.69E–02	0.09		INT or N-type
		AF 50	164.0	76.8	3.37E–02	0.07		Linear, no indication of R
		TT 150	188.8	72.9	2.56E–02	0.04	N?	
		TT 200	175.7	74.3	1.87E–02	0.07		
		TT 240	143.9	74.5	1.60E–02	0.05		
		TT 270	149.4	73.4	1.48E–02	0.09		
		TT 300	163.9	75.5	1.14E–02	0.18		
		TT 330	180.4	76.9	1.19E–02	0.09		
		TT 360	160.7	74.6	1.17E–02	0.08		
		TT 400	187.4	70.5	1.33E–02	0.07		
18X-3, 110	160.200							
		NRM 0	149.8	83.9	3.42E–02	0.13		
		AF 50	186.0	82.4	1.06E–02	0.22		Steep down, INT
		TT 150	184.3	67.3	6.74E–03	0.17		
		TT 150	173.4	63.3	6.88E–03	0.26		
		TT 200	218.2	65.1	4.38E–03	0.27		Weak after 150°C
		TT 200	222.6	61.5	4.11E–03	0.29		Stable DII, no decay
		TT 240	217.4	60.3	4.25E–03	0.19	N?	
		TT 240	208.6	59.6	4.38E–03	0.18		
		TT 300	216.9	59.6	3.65E–03	0.16		
		TT 300	204.9	66.1	3.48E–03	0.17		
18X-5, 133	163.39							
		NRM 0	177.2	78.1	5.75E–02	0.01		
		AF 50	210.7	80.5	1.42E–02	0.05		
		TT 150	132.7	77.8	1.35E–02	0.29		
		TT 150	130.8	73.0	1.01E–02	0.06		Steep down, INT
		TT 200	110.0	61.1	9.72E–03	0.17		
		TT 200	109.0	62.7	1.00E–02	0.07	NPP	
		TT 240	125.0	50.4	6.25E–03	0.21		
		TT 240	118.9	48.8	7.04E–03	0.16		
		TT 270	126.2	42.5	6.28E–03	0.35		Seems linear => N??
		TT 270	123.7	43.3	6.04E–03	0.40		
		TT 300	136.8	59.1	4.59E–03	0.43		Weak, high errors
		TT 300	146.6	62.2	4.67E–03	0.30		
		TT 330	139.5	55.9	4.11E–03	0.38		
		TT 330	135.5	52.2	3.74E–03	0.40		
		TT 360	139.5	42.6	3.19E–03	0.53		
		TT 400	108.8	52.5	4.86E–03	0.25		
		TT 400	108.6	54.0	4.51E–03	0.36		
18X-7, 24	165.3							
		NRM 0	117.3	52.6	4.82E–02	0.06		Relatively strong, and low-angle
		AF 50	107.9	29.6	2.50E–02	0.13		Looks N-type
		TT 150	121.2	19.1	2.21E–02	0.07	N (Suganuma had NP, but Jim decided to lean towards his comments)	
		TT 200	129.4	22.2	1.57E–02	0.07		
		TT 240	128.8	22.5	1.43E–02	0.05		
		TT 300	130.5	26.7	1.23E–02	0.04		

Table AT1 (continued).

Core, section, interval (cm)	Depth (mcd)	Demagnetization (mT/°C)	Declination (°)	Inclination (°)	ChRM intensity (mA/m)	Error	Polarity assignments	Comments
19X-1, 136	166.86							
		NRM 0	151.2	–29.1	2.92E–02	0.08		
		AF 50	137.6	–56.6	2.94E–02	0.04		Begins NEGATIVE
		TT 150	166.0	–63	2.45E–02	0.04		
		TT 200	174.2	–65.9	1.96E–02	0.08		General behavior looks "N"
		TT 240	153.2	–63.5	1.59E–02	0.04		Weird
		TT 270	167.3	–64.1	1.74E–02	0.12	INT	
		TT 300	181.2	–63.2	1.59E–02	0.09		
		TT 330	200.9	–61.9	1.28E–02	0.09		
		TT 360	184.8	–70.6	9.81E–03	0.13		
		TT 400	199.3	–65.7	9.28E–03	0.11		
20X-1, 26	175.46							
		NRM 0	345.1	53.5	1.62E–01	0.10		
		AF 50	346.9	37.7	8.17E–02	0.11		Nice N, essentially stable Decl NRM to 240°C
		TT 150	343.0	38.1	6.08E–02	0.07	N	
		TT 200	341.6	37.1	5.55E–02	0.10		
		TT 240	340.8	38.6	5.39E–02	0.05		
		TT 300	334.7	35.2	4.46E–02	0.06		

Notes: NRM = natural remanent magnetization, AF = alternating-field demagnetization, TT = thermal demagnetization. Characteristic direction polarity ratings: N or R = well-defined directions computed from at least three vectors, NP or RP = less precise directions computed from only two vectors or a suite of vectors displaying high dispersion, NPP or RPP = samples that did not achieve adequate cleaning during demagnetization but their polarity was obvious, N?? or R?? = uncertain, INT = indeterminate.

Table AT2. Late Eocene–Albian paleomagnetic analysis, Hole 1257B. (This table is available in an **oversized format.**)

Table AT3. Maastrichtian–Campanian paleomagnetic analysis, Hole 1257C. (See table notes. Continued on next page.)

Core, section, interval (cm)	Depth (mcd)	Demagnetization (mT/°C)	Declination (°)	Inclination (°)	ChRM intensity (mA/m)	Error	Polarity assignments	Comments
207–1257C–								
7R–5, 130	148.76							
		NRM 0	330.9	50.7	1.52E–02	0.08		Hook–type swing in declination
		AF 50	331.0	19.9	6.23E–03	0.09	RP	
		AF 50	328.0	16.6	6.24E–03	0.07		
		TT 150	226.3	51.6	1.28E–02	0.07	C31r	
		TT 150	223.2	50.5	1.18E–02	0.04		
		TT 200	118.3	52.1	3.34E–03	0.17		
		TT 200	128.7	48.1	3.20E–03	0.11		
		TT 250	142.6	19.8	5.04E–03	0.09		
		TT 250	137.5	24.8	5.45E–03	0.21		
		TT 300	137.9	29.9	3.69E–03	0.19		
		TT 300	138.1	36.3	3.90E–03	0.22		
		TT 350	198.8	4.6	3.61E–03	0.09		
		TT 350	212.4	–0.4	3.85E–03	0.07		
9R–1, 80	161.91							
		NRM 0	63.3	27.0	2.02E–01	0.04		
		AF 50	57.3	24.6	1.55E–01	0.06		N–type
		TT 150	55.2	20.9	1.32E–01	0.04		relatively strong
		TT 200	51.4	21.0	1.08E–01	0.06	NP	
		TT 240	51.4	18.0	1.01E–01	0.05		
		TT 270	51.1	20.1	1.01E–01	0.04	C32n	
		TT 300	49.0	22.7	7.44E–02	0.05		
		TT 330	53.4	12.9	6.29E–02	0.05		
		TT 360	46.4	8.2	4.56E–02	0.05		
		TT 400	44.8	17.0	4.86E–02	0.04		
9R–3, 84	164.95							
		NRM 0	61.9	41.9	5.35E–02	0.05		N–type
		NRM 0	61.9	41.9	5.35E–02	0.05	NP	
		AF 50	45.6	34.1	3.35E–02	0.04		
		AF 50	45.6	34.1	3.35E–02	0.04		
		TT 150	39.3	28.2	2.56E–02	0.11		
		TT 150	39.3	28.2	2.56E–02	0.11		
		TT 200	36.3	35.8	1.54E–02	0.21		
		TT 200	36.3	35.8	1.54E–02	0.21		
		TT 240	36.6	39.5	1.59E–02	0.06		
		TT 240	36.6	39.5	1.59E–02	0.06		
		TT 300	33.4	33.4	1.41E–02	0.06		
		TT 300	33.4	33.4	1.41E–02	0.06		
9R–5, 41	167.46							
		NRM 0	245.0	31.7	4.25E–02	0.14		Hook–type
		AF 50	244.2	7.5	4.78E–02	0.04	RP	
		TT 150	235.6	6.4	6.13E–02	0.12		
		TT 200	237.9	2.5	5.94E–02	0.07	C32r	
		TT 240	242.7	–3.8	5.70E–02	0.09		
		TT 300	234.2	–3.4	4.68E–02	0.04		

Table AT3 (continued).

Core, section, interval (cm)	Depth (mcd)	Demagnetization (mT/°C)	Declination (°)	Inclination (°)	ChRM intensity (mA/m)	Error	Polarity assignments	Comments
9R–6,59	168.64							
		NRM 0	270.5	78.8	1.65E–01	0.02		Begins steep down
		AF 50	309.4	69.9	8.75E–02	0.01		Sort–of–hook
		TT 150	323.7	61.5	6.93E–02	0.08	RP	
		TT 200	335.8	37.8	4.63E–02	0.05		
		TT 240	339.0	36.1	4.06E–02	0.05		
		TT 270	338.1	36.0	3.76E–02	0.04		
		TT 300	333.2	14.9	2.98E–02	0.08		
		TT 300	331.7	14.1	3.00E–02	0.07		
		TT 330	328.1	0.5	2.25E–02	0.09		
		TT 360	334.3	0.0	2.33E–02	0.08		
		TT 400	335.8	8.3	2.25E–02	0.06		

Notes: NRM = natural remanent magnetization, AF = alternating–field demagnetization, TT = thermal demagnetization. Characteristic direction polarity ratings: NP or RP = less precise directions computed from only two vectors or a suite of vectors displaying high dispersion.

Table AT4. Paleomagnetic analysis, Hole 1258A. (This table is available in an **oversized format.**)

Table AT5. Paleomagnetic analysis, Hole 1258B. (This table is available in an **oversized format.**)

Table AT6. Paleomagnetic analysis, Hole 1259A. (This table is available in an **oversized format.**)

Table AT7. Paleomagnetic analysis, Hole 1259B. (This table is available in an **oversized format.**)

Table AT8. Paleomagnetic analysis, Hole 1260A. (See table notes. Continued on next four pages.)

Core, section, interval (cm)	Depth (mcd)	Demagnetization (mT/°C)	Declination (°)	Inclination (°)	ChRM intensity (mA/m)	Error	Polarity assignments	Comments
207-1260A-								
17R-1,86	143.25							Hook-type
		NRM 0	62.1	30.7	2.20E–02	0.06	R	
		AF 50	68.9	11.1	2.46E–02	0.09		
		TT 150	68.7	10.8	2.48E–02	0.02		
		TT 200	71.1	2.9	2.63E–02	0.04		
		TT 250	70.0	7.2	2.51E–02	0.03	C20r	
		TT 300	69.7	2.4	2.20E–02	0.06		
		TT 350	66.7	0.6	1.73E–02	0.26		
		TT 400	73.1	1.2	1.75E–02	0.07		
17R-3, 43	145.82							
		NRM 0	11.1	39.7	1.87E–02	0.07		Hook-type
		AF 50	23.8	19.3	1.89E–02	0.05	R	
		TT 150	24.6	14.2	2.05E–02	0.07		
		TT 200	25.8	5.3	2.22E–02	0.02		
		TT 250	27.8	4.2	2.05E–02	0.02		
		TT 300	27.7	5.8	1.89E–02	0.04		
		TT 350	24.6	12.7	1.60E–02	0.20		
		TT 400	26.6	5.7	1.35E–02	0.09		
18R-1, 42	152.11							
		NRM 0	303.1	20.3	1.60E–02	0.02		Hook-type
		AF 50	292.2	12.5	1.82E–02	0.07	R	
		TT 150	268.5	5.5	1.79E–02	0.05		
		TT 200	283.9	0.8	2.02E–02	0.06		
		TT 250	284.3	2.8	1.75E–02	0.07		
		TT 300	281.5	–0.7	1.65E–02	0.10		
		TT 350	284.5	7.7	1.32E–02	0.05		
		TT 400	283.3	2.4	1.20E–02	0.04		
18R-3, 61	155.30							
		NRM 0	210.5	51.8	8.39E–03	0.13		Nice hook!
		AF 50	205.1	23.5	1.08E–02	0.05	R	
		TT 150	194.0	20.2	1.56E–02	0.10		
		TT 200	205.1	7.6	1.40E–02	0.06		
		TT 250	210.6	1.5	1.21E–02	0.05	(near 180; horiz)	
		TT 300	209.9	3.2	1.02E–02	0.08		
		TT 350	203.0	3.1	8.45E–03	0.10		
		TT 400	200.1	10.2	6.51E–03	0.05		
18R-5, 15	157.84							
		NRM 0	321.9	6.1	4.06E–02	0.04		Hook-type
		AF 50	319.9	4.8	4.24E–02	0.02		Increases intensity to TT50
		TT 150	321.1	2.5	4.26E–02	0.03	R	
		TT 200	319.9	–3.2	4.39E–02	0.04		
		TT 250	320.9	–0.9	3.91E–02	0.01		
		TT 300	319.8	–1.9	3.58E–02	0.03		
		TT 350	319.8	0.8	2.93E–02	0.03		
		TT 400	318.6	–4.4	2.57E–02	0.04		
18R-7, 63	161.32							
		NRM 0	318.3	31.2	2.65E–02	0.04		Hook-type
		AF 50	318.5	22.2	2.69E–02	0.06	R	

Table AT8 (continued).

Core, section, interval (cm)	Depth (mcd)	Demagnetization (mT/°C)	Declination (°)	Inclination (°)	ChRM intensity (mA/m)	Error	Polarity assignments	Comments
		TT 150	320.3	25.2	2.45E–02	0.06		
		TT 200	338.3	4.8	2.91E–02	0.02		
		TT 250	338.3	4.6	2.53E–02	0.03		
		TT 300	337.6	4.6	2.23E–02	0.04		
		TT 350	337.6	4.0	1.90E–02	0.05		
		TT 400	337.1	–0.9	1.64E–02	0.02		
19R-1, 61	162.01							
		NRM 0	243.0	23.7	1.07E–02	0.06		Hook-type
		AF 50	224.8	10.0	1.46E–02	0.06	R	
		TT 150	221.8	6.6	1.64E–02	0.08		
		TT 200	215.2	2.6	1.62E–02	0.07		
		TT 250	219.7	3.6	1.56E–02	0.09	(near 180; horiz)	
		TT 300	217.9	1.7	1.36E–02	0.07		
		TT 350	217.1	4.7	1.05E–02	0.05		
		TT 400	216.3	1.9	1.03E–02	0.03		
19R-3, 95	165.34							
		NRM 0	188.8	57.0	1.19E–02	0.06		Hook-type
		AF 50	171.0	22.4	1.45E–02	0.05	R	
		TT 150	177.9	16.3	1.63E–02	0.03		
		TT 200	175.6	7.8	1.78E–02	0.04	C20r	
		TT 250	175.4	8.6	1.57E–02	0.03		
		TT 300	178.9	3.1	1.47E–02	0.05	(near 180; horiz)	
		TT 350	173.7	2.2	1.30E–02	0.04		
		TT 400	171.9	1.5	1.16E–02	0.02		
20R-1, 30	171.29							
		NRM 0	111.4	4.7	1.93E–02	0.04		Hook-type
		AF 50	120.9	0.3	2.47E–02	0.03	R	
		TT 150	124.4	–6.2	2.63E–02	0.03		
		TT 200	124.6	–1.5	2.46E–02	0.03		
		TT 250	122.4	–0.1	2.21E–02	0.04		
		TT 300	126.3	–6.3	2.05E–02	0.05		
		TT 350	121.7	–6.2	1.66E–02	0.04		
		TT 400	125.4	–2.9	1.51E–02	0.02		
20R-3, 130	175.29							
		NRM 0	64.0	5.7	4.12E–02	0.06		N-type
		AF 50	70.1	1.3	3.01E–02	0.07	N	
		TT 150	72.1	3.8	2.78E–02	0.05		
		TT 200	73.1	–2.8	2.25E–02	0.09		
		TT 250	74.4	–7.5	2.27E–02	0.05	C21n	
		TT 300	75.8	–3.1	2.20E–02	0.09		
		TT 350	76.5	–10.8	2.03E–02	0.03		
		TT 400	75.5	–7.4	1.79E–02	0.08		
20R5, 62	177.61							
		NRM 0	61.6	7.0	4.96E–02	0.07		N-type
		AF 50	66.2	–0.2	4.08E–02	0.08	N	
		TT 150	68.2	–0.7	3.64E–02	0.07		
		TT 200	69.9	–3.2	2.96E–02	0.08		
		TT 250	69.7	–4.4	2.86E–02	0.06		
		TT 300	69.1	–7.2	2.61E–02	0.03		

Table AT8 (continued).

Core, section, interval (cm)	Depth (mcd)	Demagnetization (mT/°C)	Declination (°)	Inclination (°)	ChRM intensity (mA/m)	Error	Polarity assignments	Comments
		TT 350	70.9	–9.6	2.21E–02	0.04		
		TT 400	69.8	–8.7	2.03E–02	0.02		
21R-1, 28	180.98							
		NRM 0	195.0	2.4	3.51E–02	0.04		N-type
		AF 50	195.8	1.9	3.12E–02	0.04	N	
		TT 150	197.0	–3.8	3.02E–02	0.05		
		TT 200	193.5	–6.6	2.45E–02	0.07	(near 180; horiz)	
		TT 250	194.1	–7.1	2.31E–02	0.02		
		TT 300	196.2	–6.1	2.15E–02	0.04		
		TT 350	192.4	–9.7	2.02E–02	0.04		
		TT 400	189.6	–6.9	1.93E–02	0.03		
23R-1, 58	200.17							
		NRM 0	358.3	37.7	8.60E–01	0.03		Some decl swing; more hook-like than N-type
		AF 50	305.9	23.6	6.69E–01	0.06	NPP	
		TT 150	294.7	18.2	5.53E–01	0.06		
		TT 200	292.8	15.6	5.64E–01	0.01		
		TT 250	292.5	12.3	5.14E–01	0.05		
		TT 300	290.1	13.9	4.52E–01	0.03	probably still C21n	
		TT 350	290.0	14.7	4.10E–01	0.06		
		TT 400	289.8	14.7	3.68E–01	0.01		
23R-3, 43	203.02							
		NRM 0	211.3	17.1	1.10E+00	0.05	NPP	
		AF 50	207.6	0.8	1.15E+00	0.06		Somewhat hook-type
		TT 150	206.5	1.2	9.54E–01	0.03		but lot of "N" appearance
		TT 200	205.7	0.8	8.22E–01	0.04		
		TT 250	204.8	–0.1	7.22E–01	0.05	(near 180; horiz)	
		TT 300	204.0	2.2	6.32E–01	0.02		
		TT 350	204.2	1.8	5.97E–01	0.02		
		TT 400	205.3	1.5	5.39E–01	0.03		
24R-1, 6	209.35							
		NRM 0	167.1	35.1	1.93E–01	0.05		Hook-type
		AF 50	168.9	17.9	2.01E–01	0.04	R	
		TT 150	169.5	13.9	2.02E–01	0.03		
		TT 200	169.9	7.8	2.05E–01	0.02		
		TT 250	169.6	6.6	1.97E–01	0.02		
		TT 300	168.5	6.0	1.80E–01	0.02		
		TT 350	170.1	5.1	1.58E–01	0.03	C21r	
		TT 400	170.2	6.3	1.45E–01	0.02		
24R-3, 35	212.44							
		NRM 0	344.6	22.0	2.37E+00	0.01		Swing in decl
		AF 50	15.6	21.5	1.19E+00	0.04		Hook-type
		TT 150	42.0	18.2	9.51E–01	0.03	R	
		TT 200	46.6	17.8	9.61E–01	0.07		
		TT 250	52.3	13.0	9.30E–01	0.01		
		TT 300	54.2	16.0	7.68E–01	0.08		
		TT 350	54.7	11.7	6.88E–01	0.07		
		TT 400	56.7	13.5	6.16E–01	0.10		

Table AT8 (continued).

Core, section, interval (cm)	Depth (mcd)	Demagnetization (mT/°C)	Declination (°)	Inclination (°)	ChRM intensity (mA/m)	Error	Polarity assignments	Comments
24R-5, 31	215.29							
		NRM 0	84.5	14.7	2.09E+00	0.06		Midway between N-type and hook-type
		AF 50	99.3	5.1	1.58E+00	0.08	R??	
		TT 150	106.9	5.2	1.19E+00	0.06		
		TT 200	106.5	5.7	1.03E+00	0.06		
		TT 250	107.1	5.8	8.88E–01	0.09		
		TT 300	110.2	0.9	7.44E–01	0.02		
		TT 350	110.0	–1.8	6.75E–01	0.02		
		TT 400	111.4	2.9	6.19E–01	0.05		
25R-1, 12	219.01							
		NRM 0	13.9	22.2	1.96E+00	0.03		N-type
		AF 50	29.9	11.9	1.50E+00	0.08	N	
		TT 150	36.8	7.6	1.19E+00	0.03	top of C22n?	
		TT 200	37.2	7.6	1.10E+00	0.06		
		TT 250	37.5	5.1	9.68E–01	0.06		
		TT 300	38.6	4.8	7.75E–01	0.01		
		TT 350	38.7	4.5	6.70E–01	0.04		
		TT 400	38.7	5.1	5.95E–01	0.05		
							Biostrat gap of P9 = C22n and C22r = between 24R-CC and 25R-1, 50 cm; but uncertain about the above sample.	
25R-3, 91	222.80							
		NRM 0	343.0	17.3	5.63E+00	0.03		N-type
		AF 50	337.2	8.4	4.89E+00	0.05	N	
		TT 150	335.6	7.1	4.04E+00	0.03		
		TT 200	335.8	8.1	3.62E+00	0.03		
		TT 250	335.3	6.2	3.09E+00	0.04	lower C23n	
		TT 300	334.5	5.3	2.46E+00	0.01		
		TT 350	334.5	5.8	2.13E+00	0.02		
		TT 400	334.8	6.8	1.92E+00	0.01		
25R-5, 5	224.74							
		NRM 0	53.3	39.7	3.19E+00	0.06		N-type
		AF 50	62.6	41.3	1.18E+00	0.04	N	
		TT 150	76.5	35.9	7.50E–01	0.04		
		TT 200	77.4	25.1	6.14E–01	0.05		
		TT 250	79.3	13.0	6.42E–01	0.03		
		TT 300	82.1	10.6	5.89E–01	0.02		
		TT 350	82.1	9.4	4.96E–01	0.05		
		TT 400	82.8	6.9	4.84E–01	0.06		
25R-7, 32	227.71							
		NRM 0	355.3	47.0	2.10E+00	0.06		Nice hook-type
		AF 50	215.2	69.8	7.55E–01	0.07	R	
		TT 150	193.0	33.9	6.95E–01	0.03		
		TT 150	192.9	33.9	6.94E–01	0.07		
		TT 200	195.5	27.9	6.93E–01	0.05	C23r	
		TT 250	195.5	25.3	6.39E–01	0.06		

Table AT8 (continued).

Core, section, interval (cm)	Depth (mcd)	Demagnetization (mT/°C)	Declination (°)	Inclination (°)	ChRM intensity (mA/m)	Error	Polarity assignments	Comments
		TT 300	196.0	22.9	5.52E–01	0.05	(near 180; horiz)	
		TT 350	195.4	25.0	4.67E–01	0.06		
		TT 400	194.7	24.7	4.26E–01	0.04		

Notes: NRM = natural remanent magnetization, AF = alternating-field demagnetization, TT = thermal demagnetization. Characteristic direction polarity ratings: N or R = well-defined directions computed from at least three vectors, NPP = samples that did not achieve adequate cleaning during demagnetization but their polarity was obvious, R?? = uncertain.

Table AT9. Paleomagnetic analysis, Hole 1260B. (This table is available in an **oversized format.**)

Table AT10. Paleomagnetic analysis, Hole 1261A. (This table is available in an **oversized format.**)

Table AT11. Paleomagnetic analysis, Hole 1261B. (**See table notes.** Continued on next page.)

Core, section, interval (cm)	Depth (mcd)	Demagnetization (mT/°C)	Declination (°)	Inclination (°)	ChRM intensity (mA/m)	Error	Polarity assignments	Comments
207-1261B-								
2R-1, 25	534.85							
		NRM 0	258.5	62.4	3.63E–02	0.11		Hook-type
		AF 50	249.6	39.6	2.58E–02	0.06	NP	
		TT 150	236.2	32.8	1.50E–02	0.08		
		TT 200	238.9	39.3	7.97E–03	0.13		
		TT 250	250.5	41.4	4.66E–03	0.32		
		TT 250	244.9	41.6	4.98E–03	0.26		
		TT 300	239.1	51.4	3.13E–03	0.38		
		TT 300	234.5	46.8	3.29E–03	0.36		
2R-3, 72	538.32							
		NRM 0	348.9	51.1	5.32E–02	0.04		Nice hook-type
		AF 50	344.5	49.6	3.01E–02	0.05	RPP	
		TT 150	317.4	74.4	1.37E–02	0.1		Flip in declination
		TT 200	191.0	53.7	8.60E–03	0.12		
		TT 250	186.4	19.8	7.89E–03	0.14		
		TT 300	180.6	1.9	7.08E–03	0.16		
2R-3, 117	538.77							
		NRM 0	87.7	55.9	3.67E–02	0.07		
		AF 50	92.5	36.1	2.37E–02	0.05		Maybe hook-type
		TT 150	99.9	36.2	9.96E–03	0.09		Very weak!
		TT 200	62.6	78.9	3.34E–03	0.21	RPP	
		TT 200	58.2	82.0	3.26E–03	0.15		
		TT 250	307.8	53.4	2.45E–03	0.3		Dead
		TT 250	317.0	61.1	2.37E–03	0.32		
		TT 300	306.0	32.8	1.36E–03	0.89		
		TT 300	282.1	50.4	4.62E–03	0.56		
		TT 350	225.4	–34	2.22E–03	0.34		
		TT 350	231.5	–37.9	2.39E–03	0.15		
3R-1, 79	541.87							
		NRM 0	40.3	57.9	2.65E–02	0.01		
		AF 50	42.7	44.3	1.61E–02	0.03		Uncertain
		TT 150	53.1	46.8	8.17E–03	0.07	N? (NRM-200 only)	
		TT 150	51.2	48.7	8.33E–03	0.04		
		TT 200	34.2	65.6	3.38E–03	0.18		
		TT 200	334.9	51.3	2.25E–03	0.47		Dead
		TT 240	52.3	60.2	3.11E–03	0.37		
		TT 240	39.3	62.0	3.12E–03	0.42		
		TT 270	46.5	48.9	1.72E–03	0.5		
		TT 270	52.6	41.6	1.52E–03	0.57		
		TT 300	47.7	16.5	1.64E–03	0.75		
		TT 300	56.4	23.8	1.81E–03	0.54		
		TT 330	2.3	58.8	2.46E–03	0.35		
		TT 330	19.6	59.7	1.98E–03	0.35		
		TT 360	322.8	11.7	1.19E–03	1.46		
		TT 360	18.8	–61.3	1.95E–03	1.47		
3R-3, 58	544.66							
		NRM 0	245.4	68.4	1.26E–02	0.21	NP	
		AF 50	252.6	49.9	1.05E–02	0.11		Seems mainly linear; no significant hook

Table AT11 (continued).

Core, section, interval (cm)	Depth (mcd)	Demagnetization (mT/°C)	Declination (°)	Inclination (°)	ChRM intensity (mA/m)	Error	Polarity assignments	Comments
		TT 150	235.0	44.4	6.89E–03	0.1		
		TT 200	229.1	49.6	4.45E–03	0.12		
		TT 200	228.7	52.8	4.58E–03	0.15		
		TT 250	229.1	45.2	2.15E–03	0.32		
		TT 250	247.2	49.7	2.35E–03	0.28		
3R-5, 58	547.74							
		NRM 0	287.0	69.8	1.44E–02	0.12		
		AF 50	259.9	57.4	7.38E–03	0.07		Hook-type; but weak
		TT 150	246.9	69.3	4.25E–03	0.18	RPP	
		TT 150	265.1	68.5	4.12E–03	0.16		
		TT 200	27.8	67.7	3.15E–03	0.33		
		TT 200	29.1	75.7	3.35E–03	0.22		
		TT 250	45.4	54.2	2.26E–03	0.38		
		TT 250	40.0	47.5	2.54E–03	0.38		
4R-1, 59	550.83							
		NRM 0	214.3	58.5	3.71E–02	0.14		
		AF 50	201.9	55.8	1.85E–02	0.1		Steep, but looks like hook-type behavior
		TT 150	225.9	67.7	1.18E–02	0.13	RPP	
		TT 200	301.9	64.4	5.09E–03	0.22		
		TT 200	294.2	57.6	4.98E–03	0.26		
		TT 240	321.8	63.1	6.19E–03	0.3		
		TT 240	334.1	68.2	5.60E–03	0.25		
		TT 270	306.4	41.0	3.81E–03	0.55		
		TT 270	299.5	40.8	4.12E–03	0.5		
		TT 300	336.9	19.7	2.97E–03	0.66		
		TT 300	338.7	20.3	3.26E–03	0.56		
		TT 330	18.1	30.5	3.43E–03	0.52		
		TT 330	16.8	33.8	3.62E–03	0.47		
		TT 360	19.5	1.1	2.85E–03	1.32		
		TT 360	24.5	13.1	2.99E–03	0.91		
4R-3, 62	553.86							
		NRM 0	172.5	67.5	1.39E–02	0.04		
		AF 50	240.7	76.6	1.51E–02	0.07		Looks hook-type
		TT 150	243.4	34.7	7.95E–03	0.12	RP	
		TT 150	243.3	35.4	8.28E–03	0.15		
		TT 200	280.1	30.0	5.74E–03	0.19		
		TT 200	280.1	27.2	6.16E–03	0.22		
		TT 250	292.6	20.6	4.78E–03	0.23		
		TT 250	288.5	18.0	4.45E–03	0.2		
		TT 300	279.8	17.7	3.81E–03	0.07		
		TT 300	280.5	22.8	4.35E–03	0.13		

Notes: NRM = natural remanent magnetization, AF = alternating-field demagnetization, TT = thermal demagnetization. Characteristic direction polarity ratings: N = well-defined directions computed from at least three vectors, NP or RP = less precise directions computed from only two vectors or a suite of vectors displaying high dispersion, RPP = samples that did not achieve adequate cleaning during demagnetization but their polarity was obvious.